SILICA, VITREOUS

1. Introduction

Vitreous silica [60676-86-0] is an amorphous phase of silicon dioxide. Modern methods of manufacture use chemical precurosrs to prepare the glass, however, vitreous silica was traditionally formed by heating crystalline SiO_2 above its melting point, $1730 \pm 5^{\circ}C$ (1), and then cooling it rapidly enough to avoid recrystallization. Because molten SiO_2 is extremely viscous, glass formation is possible at a relatively slow cooling rate. Vitreous silica is available in a variety of forms, including powders, coatings, fibers, porous bodies, and bulk (dense) glass. This article focuses, for the most part, on the processing, properties, and uses of the bulk glass (see SILICA, AMORPHOUS SILICA).

Vitreous silica has a wide range of commercial and scientific applications. Its unique combination of physical properties includes good chemical resistance, minimal thermal expansion, high refractoriness, and excellent optical transmission from the deep ultraviolet (uv) to the near-infrared (ir).

Although vitreous silica is a simple, single-component glass, its properties can vary significantly, depending on thermal history, the type and concentration of defects, and the presence of dopants and impurities. Vitreous silica can, however, be one of the purest commercially available glassy materials. In synthetic vitreous silicas, eg, total metal contamination is typically measured in the 50–100 ppb range. Even at such a low level of impurities, differences in properties, eg, uv transmission, are observed for various silicas.

Vitreous silica is a difficult material to manufacture, and as such is more expensive than most commercial glasses. It has a high vapor pressure, a strong tendency to devitrify, and a high viscosity even at its melting point. These physical characteristics preclude the use of standard glass-forming techniques. For optical-quality glass in particular, there is a need to maintain high purity and obtain excellent homogeneity of the refractive index; these specifications have, in part, led to the development of several unique manufacturing approaches, eg, electric fusion and flame hydrolysis.

Vitreous silica is known largely as a synthetic material, but there are instances of the material occurring in nature (2,3). Vitreous tubes called fulgurites are produced when lightning fuses quartz sand. Large deposits of fulgurite exist in the Libyan desert. Vitreous silica can also be produced by meteor impact. The impact leads to rapid adiabatic heating of the quartz above its melting point. The quartz forms a glass on cooling. Examples of this type of vitreous silica have been found near Canyon Diablo, Arizona, and in meteorite craters in Australia and Arabia.

Vitreous silica is known by a number of names, most of which were developed to describe vitreous silicas formed using a particular processing method (4–6). These names are often misapplied as generic names for all vitreous silicas. Silica (qv) is a general term that refers to all forms of silicon dioxide, both crystalline and glassy; silica glass is an ambiguous term because it sometimes refers to any silica-containing glass composition; fused silica applies to vitreous silicas formed by fusion; fused quartz refers to vitreous silica formed specifically by the direct melting of quartz crystals; and synthetic fused silica describes vitreous silicas formed from chemical precursors, such as silicon tetrachloride. Uses

of the terms quartz and quartz glass should normally be avoided. These confuse vitreous silica with quartz, a crystalline form of silicon dioxide.

The optical quality of vitreous silica can range from transparent to opaque. Opaque glass contains a large number of isolated bubbles ranging in size from 5 to 200 μm (7). The bubbles scatter light, giving the glass a milky appearance. This material, produced by melting quartz sand, also tends to be less pure (99.5–99.9 wt% SiO_2) than more transparent materials. The opaque glass is an inexpensive form of vitreous silica and is often used where purity and optical properties are not important.

Transparent vitreous silicas have historically been classified by an informal scheme that differentiates the glasses by manufacturing method (8–10). Five general types of commercial glasses are listed in Table 1. Although this list gives a good overview of the available glasses, it is not complete. Many of the listed manufacturing methods have processing variations that can alter glass chemistry and properties. Moreover, the Type V designation is not as widely recognized as the others. Also, the list does not include the hybrid processes that combine some of the key features of different methods. For example, there have been efforts to produce glass by flame-fusing sol–gel produced powder (11).

2. Structure

Vitreous silica is considered the model glass-forming material, and as a result has been the subject of a large number of X-ray, neutron, and electron diffraction studies (12–16). These investigations provide a detailed picture of the short-range structure in vitreous silica, but questions about the long-range structure remain.

The basic structural element in both vitreous and crystalline silica is the SiO_4^{4-} tetrahedron, which arises from the sp^3 hybrid orbitals of the silicon. Each silicon atom sits in the center of the tetrahedron surrounded by four oxygen atoms that hold the corner positions. Tetrahedrons bond together by corner sharing. In a properly developed structure, each oxygen is shared by only two tetrahedrons. This bonding scheme can produce a large variety of three-dimensional (3D) structures and is the reason that silica has a number of crystalline phases.

The bonding scheme can also accommodate a large degree of disorder without breaking the Si–O links. Diffraction studies on vitreous silica show that the randomness of the structure results from variations in the Si–O–Si bond angle. The individual SiO_4^{4-} units do not show significant distortion. The O–Si–O bond angle is fixed at 109.5°, expected in a symmetric tetrahedral configuration, and the Si–O bond distance, 161 pm, is the same as that observed in the crystalline silica phases. The Si–O–Si bond angles, on the other hand, show a distribution that varies from 120 to 180°. Whereas original analysis of the X-ray measurements placed the maximum of the angle distribution at ~144°, a more recent reexamination of the data showed the most probable bond angle to be 152° (17). High temperature X-ray measurements show that the bond distances are constant up to 1000°C (18).

In the crystalline form of silica, the SiO_4^{4-} tetrahedrons link together in a series of interconnecting, six-membered rings. In the glassy form, the tetrahedral

network can be modeled using a distribution of ring sizes normally ranging from three- to eight-membered units (19). The six-membered ring is the most common size but it can exist in distorted configurations which are not present in the crystalline structures. Detailed ring statistics of the glassy phase cannot be extracted directly from diffraction data. The three- and four-membered rings have been studied using Raman scattering (20,21).

The longer range structure of vitreous silica has been the subject of much debate. Two basic models have been presented (14,22,23). The random network model assumes that the SiO_4^{4-} tetrahedrons are connected in a completely random fashion and that there are no ordered microregions. The crystallite-based models argue that vitreous silica consists of very small, randomly oriented microcrystals. These regions are assumed to be 0.7–2.0 nm in size and connected by noncrystalline boundary regions. One problem of the crystallite models is that, because of the small sizes proposed for the crystallites, the fraction of atoms in the boundary regions should be significant and include species, eg, $O_S{=}Si$ double bond, where O_S signifies an oxygen on the surface of the crystallite. There are, however, no indications of large concentrations of these species in the diffraction and vibrational spectra in as-formed vitreous silica (24,25). As a counterpoint, several researchers have suggested that the anomalous changes seen in a number of the physical properties of vitreous silica near the transformation temperatures of the crystalline phases occur because the atomic arrangements present in vitreous silica relate, to some extent, to crystalline structures (26).

The tetrahedral network can be considered the idealized structure of vitreous silica. Disorder is present, but the basic bonding scheme is still intact. An additional level of disorder occurs because the atomic arrangement can deviate from the fully bonded, stoichiometric form through the introduction of intrinsic (structural) defects, dopants, and impurities. These perturbations in the structure have significant effects on many of the physical properties. A key concern is whether any of these entities breaks the Si–O bonds that hold the tetrahedral network together. Fracturing these links produces a less viscous structure that can respond more readily to thermal and mechanical changes.

The intrinsic defects include paramagnetic and diamagnetic species (24,27,28). The paramagnetic defects have received the most study because they are readily detectable by electron spin resonance (esr) spectrometry. Paramagnetic defects that have been identified by esr include the E' center, the nonbridging oxygen hole center; and the peroxyl radical. All of these defects are normally induced in vitreous silica by ionizing radiation or uv light.

A number of diamagnetic defects are also believed to exist in vitreous silica. Because there is no direct way to study these species, their identification is either done indirectly, eg, by uv absorption, or by employing esr after the material has been made paramagnetic using ionizing or laser irradiation. The proposed diamagnetic species include the neutral oxygen vacancy, the doubly coordinated silicon, and the peroxyl bond. The diamagnetic defects occur when the glass-forming conditions are off-stoichiometry.

The impurity (extrinsic) defects include nonmetallic and metallic additives or contaminanats (29–32). The nonmetallic contaminants are the more prevalent type in most high grade vitreous silicas. In the synthetic silicas, eg, the concentrations of nonmetallics can be three to five orders of magnitude higher than that

of metallics. The nonmetallic contaminants include species, eg, hydrogen, chlorine, fluorine, and oxygen, which can be present in the furnace atmosphere during certain forming, consolidation, or special annealing treatments. These impurities exist in the vitreous silica in a variety of forms. They can link directly to the silica network, eg, hydroxyl, Si−OH bonding; hydride, Si−H, bonding; and chloride, Si−Cl, bonding; or exist interstitially as molecular species, such as H_2, H_2O, Cl_2, and O_2. Metallic contaminants are usually picked up from the silica raw material or from the furnace materials during processing. These dissolve in the silica network by bonding in some way to the oxygen ions. Table 2 lists the metal impurities commonly seen in vitreous silicas.

3. Manufacturing

Vitreous silica, a hard glass having a limited working range, is not conventionally produced using conventional glass-melting techniques. Rather, its high melting point and high melt viscosity have forced the development of a number of unique forming methods that utilize sintering or some type of deposition process. Many of the key physical properties depend on the specific forming process used because the forming process defines the material's thermal history and impurity–dopant profile. However, in most cases these developments have led to very high purity glasses with high index homogeneity and other properties that can be largely engineered.

3.1. History. The first reported instances of fusing silicon dioxide occurred early in the nineteenth century. In 1813, fusing of small crystals of quartz by injecting oxygen into an alcohol flame was described. This was followed in 1821 by the description of the fusing of quartz crystals using a hydrogen–oxygen torch (33). Properties of vitreous silica were first measured in 1839 (34). A glass produced using a hydrogen–oxygen flame exhibited remarkable strength, good elasticity, and excellent thermal shock resistance. This glass also had a tendency to volatilize and to devitrify. Later, the glass was shaped into tubes and bulbs. In 1887, a flame was used to draw fibers of vitreous silica (35).

Several efforts to develop commercial processes began $\sim$ 1900 and were centered mainly in England, France, and Germany (35). It was during this early commercialization of vitreous silica that the distinction between the opaque and transparent glasses arose. The opaque material, called fused silica, was made by fusing sand. Resistance heating with carbon electrodes was an effective method for generating the desired temperature. The transparent material, called fused quartz, was made by fusing clear, selected quartz crystals. Achieving transparency by this approach required overcoming the problem of bubble formation in the glass. Crystalline quartz undergoes a transformation, ie, an inversion from its low to high crystalline form, at 575°C, which also includes a rapid volume change. If heating is not uniform, the crystals can fracture (splinter) and lead to air encapsulation and the formation of bubble lines. This problem was overcome in 1900 by using the fracturing phenomenon to produce a fine crystalline frit that could be subsequently flame fused without splintering (36,37). Fracturing was promoted by heating the quartz crystals to a red heat and

then quenching in water. An approach in which a glass boule was produced by injecting this powder into a flame was also advanced (38).

The production of vitreous silica from chemical precursors was first described in patents filed in 1934, including a fabrication method in which fine, high purity powders were produced by decomposing silanes (39). Forms were then cast from aqueous slips. More importantly, a flame hydrolysis process which used $SiCl_4$ as the chemical precursor was described (40). This latter approach led to a marked improvement in glass purity and served as the basis for the processes used in the 1990s to make synthetic vitreous silica.

3.2. Modern Manufacturing Techniques. Modern manufacturing processes of vitreous typically involve the fusion or viscous sintering of silica particles; the particles can be derived from sand crystals or are produced through a chemical process, eg, flame hydrolysis or sol–gel. In one practice of the flame hydrolysis process, the powder is produced and fused into glass a single step, without the isolation of a porous body. Dopant and additive profiles are concentration are then controlled by the deposition conditions. When a process involving a discrete porous silica body as an intermediate is used, subsequent processing steps can be used to control dopant levels and in particular, the hydroxyl level of the final glass. The choice of fabrication method is often dictated by the end-use specifications. Flame hydrolysis or similar chemical techniques that allow for the production of very high purity glass are the methods of choice for optical applications but may be economically wasteful for less demanding applications.

Translucent Vitreous Silica. Translucent vitreous silica is produced by fusion of high purity quartz sand crystals (41,42). Sand is packed around a graphite rod through which a current is passed. The resistance heating produces a plastic mass that can be blown into molds, drawn into tubing, or shaped by rolling or pressing. Separation from the graphite rod is facilitated by gaseous products formed by interfacial reaction. Because the outside is sandy, the product is known as sand-surface ware. A matte finish is obtained by mechanical buffing. A glazed surface is produced by fusing the outside surface with an electric carbon arc or flame.

The Rotosil process employed by Heraeus and Heraeus-Amersil is used for the production of tubular or cylindrical shapes. It permits greater uniformity and dimensional control than the previous process. The quartz is washed in hydrofluoric acid and distilled water to remove impurities that can promote crystallization during manufacture. The sand is then placed in a rotating horizontal steel tube where it is held at the circumference by centrifugal force. A carbon arc is passed slowly down the center of the drum to fuse the sand. A modification, using open rotating molds on a vertical axis, allows formation of crucibles, beakers, and bowls.

For refractory applications, sand of moderate purity is fused by an electric arc into an ingot. The ingot is then crushed and ground to a size suitable for injection molding or slurry casting. A variety of shapes can be produced, including bricks, nozzles, and pouring tubes. After shaping, the pieces are dried slowly and then fired at 1150–1250°C for 1–4 h. The materials have a white, opaque appearance.

Transparent Vitreous Silica. Clear, transparent, bubble-free vitreous silica may be obtained by melting natural quartz minerals by flame or plasma vapor deposition (synthetic fused silicas), and by sol–gel processing.

Fused Quartz. The fused quartz glasses correspond to the Type I and Type II vitreous silicas described in Table 1. Type I silica is made by the direct melting of quartz powder using the resistance, ie, Osram process (43), or induction-heated furnaces (44). The powder is fed into the top of a tubular furnace and melted in either a molybdenum or carbon crucible surrounded by a protective inert or reducing gas. Tubing or rod can be drawn from the bottom of the crucible. Vacuum is sometimes used prior to fusion to minimize the gas content in the pore spaces and hot pressing is sometimes applied after fusion to reduce the remaining bubbles. Type II silica is formed using a process originally developed by Heraeus. Quartz powder is fed through an oxy-hydrogen flame and collected as a dense glass on a rotating fused-quartz tube (45). The glass is withdrawn slowly from the flame as the fused quartz builds up. Chlorine can be introduced during laydown of the glass to improve glass purity. The chlorine removes metal contaminants, eg, aluminum, iron, copper, zinc, titanium, and the alkali and alkali-earth metals, by forming volatile chlorides (46).

The crystalline quartz powder is treated before use to improve purity and to eliminate the formation of gaseous inclusions during fusion. The powders are first washed in mixed acids, including hydrofluoric acid, to remove surface contaminants and then heated to at least 800°C and plunged into distilled water to promote extensive microcracking. The resulting powder is well suited for vacuum melting because it melts faster and expels gaseous impurities more completely than untreated quartz crystals.

Brazil continues to be an important source of quartz powder for fused quartz manufacturers. Namibia and the Malagasy Republic are also suppliers. In the United States, large deposits of crystalline quartz exist in West Virginia, Pennsylvania, and Missouri. Suppliers as of the mid-1990s included U.S. Silica and Unimin Corporation. Alternatives to the natural quartz powder, including fumed silica, flame-hydrolyzed soot, and sol–gel-derived powder, have also been tried as feedstock for these processes (11).

Although fused-quartz production is usually carried out above the melting point of cristobalite, powder sintering at temperatures in the range of 1400–1710°C is also possible (47). To avoid cristobalite formation (devitrification) while sintering at these temperatures, the powder must be pure, especially of alkali contaminants, and the time at temperature must be kept to a minimum. Typically, the sintering process takes no $>$15 min in the 1400–1710°C range. The sintering is usually done in a vacuum or in a helium atmosphere to minimize bubble formation.

Transparent vitreous silica crucibles can be produced by firing slip-cast pieces in a vacuum or a helium atmosphere (48,49), or in helium followed by argon (50). The crucible is usually supported on a graphite form to minimize distortion.

Synthetic Fused Silica. Synthetic silica can be prepared from a variety of volatile silicon compounds by oxidation or hydrolysis in a flame or plasma. Type III silica is made using a flame (40,51). In the United States, the flame is typically methane–oxygen. In Europe and Japan, hydrogen–oxygen flames are

preferred. Type IV silica is made with a low water, oxygen plasma (52,53). The plasma deposition process was developed as a way to produce low OH vitreous silica. In glasses made by flame hydrolysis, the OH level ranges from 800 to 1200 parts per million (ppm) depending on the flame mix. In glasses made by plasma deposition, it is typically <20 ppm.

Vitreous silicas made from chemical precursors are significantly purer than those from natural quartz powders because it is possible to purify chemical precursors to a higher degree than powders. This purity directly translates into higher uv and deep uv optical transmission of the final glass. Synthetic fused silicas can have a total metal content $< 200-300$ ppb. Any stable, silicon-containing compound having sufficient volatility can be used as a chemical precursor (40,54). Most industrial processing uses silicon tetrachloride because it is relatively inexpensive and readily available in large quantities. Environmental concerns have, however, prompted the development of synthetic fused silica made from cyclic and chained siloxane compounds (55,56). These chlorine-free precursors do not generate HCl as a manufacturing by-product (see SILICON COMPOUNDS).

In the typical flame or vapor-phase hydrolysis process, which uses $SiCl_4$ as the precursor, silicon tetrachloride vapor is fed into a flame using an oxygen carrier gas. Fine (< 50 nm) amorphous silica particles form in the flame (57).

$$SiCl_4 + 2\,H_2O \rightarrow SiO_2 + 4\,HCl$$

The water is a product of combustion of the hydrogen or methane gases. A portion of that water can also incorporated in the glass structure as SiOH.

The manufacture of vitreous silica by flame hydrolysis can be a single- or multistep process. In the single-step process, silica particles are formed and consolidated to dense glass in one operation. Consolidation takes place as the silica particles are collected on a substrate that is heated by the deposition flame. The deposition temperature is usually in excess of 1800°C. The single-step process as described here naturally yields vitreous silica that is relatively high in hydroxyl content. Further, the final material contains other combustion products depending on the flame and deposition conditions. Molecular H_2, eg, is easily incorporated in the glass using this process. In a two-step process, the silica is formed as a soot that can be collected as a powder or porous preform (low temperature deposition) and consolidated to dense glass in a separate operation. Consolidation is usually done at 1400–1700°C. The two-step process, although more involved, offers several advantages, including the ability to chemically treat the silica soot before final consolidation and to control the consolidation atmosphere. For example, high purity, low OH vitreous silica can be made by chemically drying the porous preform in chlorine (58) or $SOCl_2$ (59) and then consolidating in a moisture-free atmosphere. This operation is a key step in the production of optical waveguide fibers, which require low OH for ir transmission, but can also be used to manufacture bulk glass (60,61).

In the plasma deposition process, silicon tetrachloride vapor is passed through an induction-coupled plasma torch using a hydrogen-free oxygen stream:

$$SiCl_4 + O_2 \rightarrow SiO_2 + 2\,Cl_2$$

The resulting silica is deposited on a refractory substrate as a clear transparent glass.

Synthetic fused silicas with low OH levels have also been made experimentally using a CO_2 laser instead of the plasma torch (62,63). The glass rate of this process, however, is at least 10 times slower than the plasma approach.

Fused silica materials obtained by the various vapor-phase methods can be formed into rods, tubing, and boules. The pieces may range in size up to hundreds of kilograms. Any of these may be subsequently reworked to make a variety of useful products. Crucibles have been made from both tubing and massive pieces. Optical elements are cut from the boules and polished, and often finely annealed to control refractive index and reduce internal stress.

Sol–Gel Processing. Sol–gel processing is essentially a lower temperature alternative for fabricating synthetic fused silica (64–70). The starting material is either a particulate gel made by mixing fumed or colloidal silica in an appropriate liquid or a solution of a silicon alkoxide, such as tetraethylorthosilicate (TEOS) or silicon tetramethoxide, in alcohol using a controlled amount of water that hydrolyzes slowly to form a gel. After the gel is dried, it can be sintered under vacuum or in helium atmosphere to transparent vitreous silica at temperatures of 1200–1400°C. Steps are often taken to minimize the OH and chlorine content of the preforms to avoid bubble formation during sintering (71,72).

The gel approach offers processing advantages that are not available with the more conventional methods used to form synthetic fused silica. The lower firing temperatures reduce energy consumption and minimize the pickup of furnace impurities. Also, near-net-shaping is possible because the gelling procedure is not limited to any particular mold configuration. Unfortunately, the gel approach has critical drying and shrinkage problems that have thus far limited the glass sizes that can be produced. The gels, fragile structures that tend to crack during drying owing to capillary stresses, are highly porous structures that shrink linearly by up to 50% upon firing. The high shrinkage makes dimension control difficult. These problems have been attacked with limited success by increasing gel strength through gel aging, additions of silica particle fillers, etc; controlling the pore size in the gel through pH control and hydrothermal aging (73); and slower, milder drying procedures (see HYDROTHERMAL PROCESSING; SOL–GEL TECHNOLOGY). In response to these processing limitations, several hybrid processes have been proposed that use sol–gel derived powders as the feedstock for more conventional manufacturing approaches, including flame fusion and high temperature vacuum sintering (11,74).

Flame Working and Sealing. Flame working of vitreous silica is difficult because of its extremely high viscosity and volatility. However, this drawback is balanced by excellent resistance to thermal shock. Whereas a gas–oxygen flame is satisfactory for most manipulations, an oxy–hydrogen flame provides somewhat more energy. An oxy–acetylene flame gives even more heat, but promotes excessive volatilization.

When silica volatilizes, vapors condense on cooler areas to form a white bloom that can be removed by heat or dilute hydrofluoric acid. Because dilute hydrofluoric acid also attacks the substrate, a mild, careful treatment

is required. To minimize volatilization, the temperature should be as low as possible.

Annealing of flame-worked pieces is generally not necessary because of the low thermal expansion of vitreous silica. However, massive pieces should be annealed at a temperature corresponding approximately to the annealing point of the specific type and for a time determined by size. Owing to developments in applications of ir lasers (qv), vitreous silica up to 6-mm thick can be cut and drilled using CO_2 gas lasers and numerically controlled equipment. Laser cutting has the advantage over mechanical cutting of a very thin kerf (cut width) having little induced stress (75).

Vitreous silica can be attached to other glasses, eg, Corning Code 7740 borosilicate glass, using a graded seal. The silica is first sealed to Code 7230 glass having a linear expansion coefficient, α, of $\sim 14 \times 10^{-7}/^{\circ}C$, from 0 to 300°C. This in turn is sealed to Code 7240 glass, $\alpha \approx 21 \times 10^{-7}/^{\circ}C$. The assembly is then sealed to Code 7740 glass, $\alpha \approx 32.5 \times 10^{-7}/^{\circ}C$.

Sealing to metals is difficult because the thermal expansion of metals is much higher than that of vitreous silica. Nevertheless, such sealing is necessary, particularly in the case of mercury vapor lamps where vacuum-tight lead connections are required. A molybdenum foil seal is used based on the principle that a very thin foil is able to contract during cooling without inducing stress in the glass. The molybdenum foil is connected to tungsten electrodes and placed in the tube that is flushed with a neutral gas. The tube is heated strongly on the outside with a gas–oxygen flame. It collapses around the foil and is mechanically pinched to make firm contact (76).

4. Glass Properties

Vitreous silica has many exceptional properties. Most are the expected result of vitreous silica being an extremely pure and strongly bonded glass. Inert to most common chemical agents, it has a high softening point, low thermal expansion, excellent thermal shock resistance, and excellent optical transmission over a wide spectrum. Compared to other technical glasses, vitreous silica is one of the best thermal and electrical insulators and has one of the lowest indexes of refraction.

Vitreous silica, however, also exhibits a number of abnormal behaviors for a glass. These are a consequence of its inherent atomic structure (77–79). For example, the expansion coefficient is negative below approximately −80 to −100°C and positive and very small above these temperatures. In contrast to most glasses, the equilibrium density decreases with heat treatment in the transformation range. The elastic moduli increase with increasing temperatures above −190°C. The Young's modulus of vitreous silica increases linearly with applied longitudinal stress at −196°C, whereas the modulus of soda glass decreases (80). The compressibility of vitreous silica increases with pressure for pressures < 3 GPa ($< 30{,}000$ atm) and the temperature coefficient of sound velocity is positive over the range 0–800°C (81).

Discontinuities in property–temperature relationships have also been observed and are often associated with structural rearrangements seen in the

various crystalline phases of SiO_2 (26,82). The abnormalities in acoustic loss, pressure and temperature dependence of compressibility, thermal expansion, and specific heat have been related to a bimodal distribution of −Si−O−Si− bond angles (83). The large amount of free volume in the vitreous material permits reorientation of the silica tetrahedrons by changing −Si−O−Si− angles, ie, keeping Si−O distances constant, or by favoring the lower angles in the bimodal distribution.

4.1. Chemical Properties. Stoichiometric vitreous silica contains two atoms of oxygen for every one of silicon, but it is extremely doubtful if such a material really exists. In general, small amounts of impurities derived from the starting materials are present and various structural defects can be introduced, depending on the forming conditions. Water is incorporated into the glass structure as hydroxyls.

Chemical Durability. The resistance of nontransparent vitreous silica to chemical attack is slightly less than the resistance of transparent vitreous silica. This difference results primarily from the higher surface area of the former caused by the presence of a large number of bubbles. Most data in the literature are on the transparent material.

Vitreous silica does not react significantly with water under ambient conditions. The solution process involves the formation of monosilicic acid, $Si(OH)_4$. Solubility is fairly constant at low pH, but increases rapidly when the pH exceeds 9 (84–86). Above a pH of 10.7, silica dissolves mainly as soluble silicates. Solubility also increases with higher temperatures and pressures. At 200–400°C and 1–30 MPa (<10–300 atm), eg, the solubility, S, of SiO_2 in grams per kilogram (g/kg) H_2O can be expressed as follows, where d is the density of the vapor phase and T is the absolute temperature in kelvin.

$$\log S = 2 \log d - 2679/T + 4.972$$

Vitreous silica is susceptible to attack by alkaline solutions, especially at higher concentrations and temperatures. For 5% NaOH at 95°C, although crazing may be evident, surface corrosion is only 10 μm after 24 h (87). For 45 wt% NaOH at 200°C, dissolution proceeds at 0.54 mm/h (88). The corrosion rates in other alkaline solutions are listed in Table 3. Alkaline-earth ions inhibit alkaline solution attack on vitreous silica. Their presence leads to the formation of hydrated metal silicate films that protect the glass surface (89).

Vitreous silica is relatively inert to attack from most acids for temperatures up to 100°C. The weight loss data in acid solutions are summarized in Table 3. The main exceptions are phosphoric acid, which causes some corrosion above ~150°C, and hydrofluoric acid, which reacts readily at room temperature (91). This latter dissolution proceeds as follows:

$$SiO_2 + 6\,HF \rightarrow H_2SiF_6 + 2\,H_2O$$

The equilibrium constant for this reaction at 25°C is 3.4×10^{-6} (92). The effects of two hydrofluoric acid solutions of different concentrations on various silica phases are shown in Table 4.

Metals do not generally react with vitreous silica $< 1000^{\circ}C$ or their melting point, whichever is lower. Exceptions are aluminum, magnesium, and alkali metals. Aluminum readily reduces silica at 700–800°C. Alkali metal vapors attack at temperatures as low as 200°C. Sodium vapor attack involves a diffusion of sodium into the glass, followed by a reduction of the silica.

$$4\,Na + 5\,SiO_2 \rightarrow 2\,Na_2Si_2O_5 + Si^0$$

This reaction is accompanied by a blackening of the vitreous silica and a flaking of the surface. As evidence for the diffusion step, the sodium absorption by the much denser quartz is $12\,mg/(1000\,h{\cdot}cm^2)$ at 350°C, whereas vitreous silica absorbs $23\,mg/(1000\,h{\cdot}cm^2)$ at 286°C (94). Molten sodium is much less reactive.

Fused basic salts and basic oxides react with vitreous silica at elevated temperatures. Reaction with alkaline-earth oxides takes place at ~900°C. Halides tend to dissolve vitreous silica at high temperatures; fluorides are the most reactive (95). Dry halogen gases do not react with vitreous silica <300°C. Hydrogen fluoride, however, readily attacks vitreous silica.

$$SiO_2 + 4\,HF \rightarrow 2\,H_2O + SiF_4$$

Reaction with hydrogen is very slight < 500°C, but reduction does occur at higher temperatures. The formation of ≡SiOH and ≡SiH groups has been demonstrated by ir and Raman spectroscopy (96,97).

$$2\,SiO_2\,(glass) + H_2 \rightarrow \equiv SiOH + \equiv SiH$$

Vapor Pressure. Vitreous silica is a highly refractory glass. Volatilization is significant only at elevated temperatures (Fig. 1), occurring under a neutral atmosphere by dissociation.

$$SiO_2(s,l) \rightarrow SiO\,(g) + \tfrac{1}{2}O_2$$

SiO exists only as a vapor and reforms SiO_2 particles when it deposits on cold surfaces (98).

The loss of material at elevated temperatures is accelerated in vacuum and under reducing conditions. In the presence of carbon, eg, the following reaction may occur:

$$SiO_2 + C \rightarrow SiO + CO$$

For pure carbon, this reduction can take place at temperatures as low as 1200°C (95). A similar reduction occurs with tungsten, tantalum, or molybdenum in vacuum at 1300–1400°C (99).

Devitrification. At atmospheric pressure, devitrification of vitreous silica can take place at temperatures from 1000 to 1723°C, ie, the cristobalite liquidus. The maximum growth rate occurs at ~1600–1675°C (Fig. 2). Crystals form and

grow from nuclei found predominantly at the glass surface. Internal crystallization, though rarely seen, is also possible (1). Only heterogeneous nucleation has been observed as of this writing (2006), regardless of whether the crystallization occurs internally or externally. The crystalline phase, β-cristobalite, has nearly the same density and refractive index as vitreous silica. The β to α transition of cristobalite that occurs at 270°C includes a large volume change that leads to cracking and strength loss on cooling (100).

The devitrification rate is extremely sensitive to both surface and bulk impurities, especially alkali. Increased alkali levels tend to increase the devitrification rate and lower the temperature at which the maximum rate occurs. For example, a bulk level of 0.32 wt% soda increases the maximum devitrification rate 20–30 times and lowers the temperature of maximum devitrification to ~1400°C (102). The impurity effect is present even at trace levels (< 50 ppm) and can be enhanced with the addition of alumina. The devitrification rate varies inversely with the ratio of alumina-to-alkali metal oxide. The effect is a consequence of the fact that these impurities lower glass viscosity (103).

The water content and stoichiometry of the glass also influence the devitrification rate. A high hydroxyl content in the glass as well as water vapor and oxygen in the atmosphere enhance devitrification, whereas oxygen deficiency in the glass and neutral or reducing atmospheres inhibit devitrification (101,104–107). The oxygen affects the rate by diffusing through the cristobalite layer to the glass–crystal interface and oxidizing the glass, thereby bringing it closer to stoichiometry (104–106). The water vapor and hydroxyl content show a similar effect, probably by dissociating at the elevated temperatures to give free oxygen and by weakening the glass structure through the formation of silicon–hydroxyl bonds.

Increased pressures can lower the temperature at which crystallization occurs. Experiments performed using Spectrosil (Thermal Syndicate Ltd.) and G.E. Type 204 (General Electric Company) fused silicas (see Fig. 2) show that at pressures >2.5 GPa (< 25,000 atm), devitrification occurs at temperatures as low as 500°C and that at 4 GPa (< 40,000 atm), it occurs at as low as 450°C (108). Although the temperatures and pressures were in the coesite-phase field, both coesite and quartz were observed. Both the devitrification rate and the formation of the stable phase (coesite) were enhanced by the presence of water. In the 1000–1700°C region at 500–4000 MPa (< 5,000–40,000 atm), α and β quartz were the primary phases. Crystal growth rates increased with pressure and with hydroxyl content for a given stoichiometry.

Cristobalite can also form on vitreous silica at temperatures as low as 400°C when the pressure is equal to 35 MPa (< 350 atm) and the glass is immersed in weak NaOH solutions (109). In stronger NaOH solutions, quartz is formed. The formation of the crystalline phases is a result of the hydrolysis of the anions present. No crystallization occurs with HF, H_2SO_4, and H_3PO_4 in $KHSO_4$ solutions or in pure water.

Transparent silica can normally be used in air continuously at temperatures up to 1000°C and for short periods up to 1250°C without devitrification occurring. This recommendation assumes, however, that the glass surface is substantially free of alkali contamination that can occur from sources, eg, airborne dust or fingerprints.

Diffusion. The gaseous species for which diffusion parameters have been studied extensively in vitreous silica include both noble gases and molecular gases. Data are given in Table 5. In general, the activation energies for diffusion of the gaseous species scale with molecular size (110). The noble gases do not interact chemically with the glass structure. Helium is the fastest diffusing species in vitreous silica. Its diffusion coefficient over the temperature range of 24–1034°C is as follows, where T is in kelvin and R is the universal gas constant (26).

$$D_{\mathrm{He}} = 2.7 \times 10^{-7} T \exp(-4.81/RT)$$

Diffusion of the molecular gases can be complicated by reactions with the glass network, especially at the sites of structural defects. The diffusion coefficient of water, eg, shows a distinct break ~ 550°C (114). Above 550°C, the activation energy is approximately 80 kJ/mol (19 kcal/mol), but <550°C, it is only 40 kJ/mol (9.5 kcal/mol). Proposed explanations for the difference cite the fact that the reaction between water and the silica network to form hydroxyls is not in equilibrium at the lower temperatures.

The oxidation of vitreous silica appears to proceed by one of two mechanisms, depending on the material's hydroxyl content (110,115). In hydroxyl-containing material, the rapid oxidation probably occurs by the diffusion and removal of hydrogen, according to the following reaction:

$$\equiv Si^{3+}HO{-}Si^{4+}\equiv \rightarrow \equiv Si^{4+}{-}O{-}Si^{4+}\equiv + \tfrac{1}{2}H_2$$

Conversely, in hydroxyl-free vitreous silica, the oxidation is much slower and is controlled by the diffusion of oxygen through the solid according to the following reaction:

$$\equiv Si^{3+}Si^{3+}\equiv + \tfrac{1}{2}\,O_2 \rightarrow \equiv Si^{4+}{-}O{-}Si^{4+}\equiv$$

The diffusion of metal ions in vitreous silica has not been studied as extensively as that of the gaseous species. The alkali metals have received the most attention because their behavior is important in electrical applications. The diffusion coefficients for various metal ions are listed in Table 5. The general trend is for the diffusion coefficient to increase with larger ionic sizes and higher valences.

The diffusion of ^{22}Na in Infrasil fused quartz exhibits several distinct regions between 170 and 1000°C. The diffusion parameters are $D_0 = 3.44 \times 10^{-2}$ cm^2/s, and $E_d = 88.3$ kJ/mol (21.1 kcal/mol) between 573 and 1000°C; $D_0 = 0.398$ cm^2/s and $E_d = 108$ kJ/mol (25.8 kcal/mol) between 250 and 573°C; and $D_0 = 2.13$ cm^2/s and $E_d = 118$ kJ/mol (28.3 kcal/mol) between 170 and 250°C, where D_0 and E_d are the diffusion constant and activation energy of diffusion, respectively. The transitions occur at the transformation temperatures for the high–low modifications of quartz (573°C) and cristobalite (250°C), which suggests that the changes involve shifts in the specific volume of the glass structure (26,116). Diffusion data for gases in vitreous silica are listed in Table 6.

4.2. Physical Properties. *Density.* The density of transparent vitreous silica is $\sim 2.20\,g/cm^3$. Translucent and opaque glasses have lower densities owing to the entrapped bubbles. The density of translucent Vitreosil, eg, is 2.07–$2.15\,g/cm^3$ (87,120). The density of transparent vitreous silica decreases with increasing hydroxyl content and with lower fictive (glass structure equilibrium) temperatures. The fictive temperature depends on the thermal history and on glass viscosity (121).

The density of vitreous silica is lower than those of the low pressure crystalline phases of silicon dioxide (122), especially that of quartz.

Material	Density, g/cm^3
vitreous silica	2.20
cristobalite	2.27
tridymite	2.30
quartz	2.65

Because all of these structures share the same short-range bonding scheme, the density differences indicate that vitreous silica has a substantial interstitial volume and can be compacted.

A number of studies have examined the high pressure behavior of vitreous silica (123–128). The degree of compaction depends on temperature, pressure, and the time of pressurization treatment. A density increase of almost 19% was obtained when the glass was subjected to a pressure of 8 GPa (< 80,000 atm) at 575°C for 2 min. The samples remained completely amorphous, though the densities and refractive indexes were approaching those of the quartz phase (124,129). Structural studies indicate that the compaction is accompanied by a shift in the ring statistics toward a higher percentage of three- and four-membered rings of SiO_4 tetrahedrons (130). Above 20 GPa (200,000 atm), the SiO_4 tetrahedrons begin to distort and the Si coordination gradually shifts from four to six oxygens (131).

Compaction has also been observed as a result of neutron irradiation and extended exposure to intense uv (excimer) laser light (132,133). The compaction tends to relax over months at room temperature and can be reversed quickly by annealing at sufficiently high temperatures (134). Light-induced expansion of silica (an increase in its volume) has also been demonstrated, particularly in silicas that contain molecular H_2 (135,136). The effect has been correlated with the formation of SiOH and SiH under the reaction conditions (137).

Viscosity. The viscosity of vitreous silica in the transformation range depends on composition (dopants and impurities) and thermal history (26,138,139). Any additive, including OH, chlorine, fluorine, and metal ions, that can break up the Si–O–Si network lowers the viscosity. Vitreous silicas with hydroxyl levels of ~0.1 wt%, eg, Corning Code 7980, Suprasil, Spectrosil, and Dynasil, have annealing points in the 1050–1100°C range (120,140–142). Hydroxyl-free (< 0.001 wt%) high purity fused-quartz glasses, eg, ir Vitreosil, some of the General Electric types, and various Amersil grades, have softening, annealing, and strain points up to 100°C higher than those of the hydroxyl-containing

types. Thermal history determines the fictive temperature of the glass. The ir Vitreosil, which has a fictive temperature of 1400°C, has a viscosity of 1 TPa·s (=10^{13} P) at 1700°C, whereas a 1000°C fictive material has a viscosity of 1 TPa·s (=10^{13} P) at ~1320°C (138). Representative viscosity data are given in Table 7.

A complete viscosity–temperature curve is shown in Figure 3 for Amersil commercial-grade fused quartz. A number of studies have shown that, >1000°C, the viscosity, η, of vitreous silica follows the general relation

$$\ln \eta = \ln \eta_0 + E/RT$$

where η_0 is the viscosity at infinite temperature, T is temperature in kelvin, E is the activation energy, and R, the molar gas constant, is 8.31 kJ/(mol·K) (143). Typical activation energy for viscous flow ranges roughly from 450 to 550 kJ/mol (108–132 kcal/mol) for the high OH vitreous silicas.

The characteristic temperatures, ie, softening, anneal, and strain points, of vitreous silica are significantly higher than those of most commercial glasses. Vitreous silica starts to deform slowly at temperatures > 1200°C and, although it can be readily sagged at temperatures of 1400–1550°C, is a fairly viscous material even above the melting point of cristobalite [10^6–10^5 Pa·s (10^6–10^7P)]. The very high temperature viscosity data range from 930 Pa·s (9300 P) at 2085°C to 860 Pa·s (8600 P) at 3210°C (146).

4.3. Thermal Properties. *Thermal Expansion.* Most manufacturers' literature (87,120,140–142) quotes a linear expansion coefficient within the 0–300°C range of 5.4×10^{-7}–5.6×10^{-7}/°C. The effect of thermal history on low temperature expansion of Homosil (Heraeus Schott Quarzschmelze GmbH) and Osram's vitreous silicas is shown in Figure 4. The 1000, 1300, and 1720°C curves are for samples that were held at these temperatures until equilibrium density was achieved and then quenched in water. The effect of temperature on linear expansion of vitreous silica is compared with that of typical soda–lime and borosilicate glasses in Figure 5. The low thermal expansion of vitreous silica is the main reason that it has a high thermal shock resistance compared to other glasses.

Vitreous silica annealed at 1100°C has been designated NIST Standard Reference Material 739 (L1 and L2). Its expansion coefficient, α, may be calculated for 300–700 K from the following expression (148), where T is the absolute temperature in kelvin.

$$\alpha \times 10^6 = -0.8218 + 7.606 \times 10^{-3}T - 1.266 \times 10^{-5}T^2 + 6.487 \times 10^{-9}T^3$$

Precise measurements of the dimensional stability of low expansion materials indicate that vitreous silicas, eg, Corning 7980 and Homosil, display a length change at 25°C of ~0.5 parts per billion (ppb) per day (149).

The expansion coefficient of vitreous silica can be controlled by doping the glass with titania. At 7.4 wt% TiO_2, the room temperature expansion coefficient is effectively zero (<10^{-8}/°C) (150).

Heat Capacity. The mean heat capacity (0–900°C) at constant pressure, C_p, in J/(kg·°C), can be estimated in vitreous silica using the following expression, where t is temperature in degrees celsius.

$$C_p = 700 + 0.79\,t - 5.23 \times 10^{-4} t^2$$

Its value at 25°C is 0.71 J/(g·°C) [0.17 cal/(g·°C)] (95,151). Discontinuities in the temperature dependence of the heat capacity have been attributed to structural changes, eg, crystallization and annealing effects, in the glass. The heat capacity varies weakly with OH content. Increasing the OH level from 0.0003 to 0.12 wt% reduces the heat capacity by approximately 0.5% at 300 K and by 1.6% at 700 K (152). The low temperature (< 10 K) heat capacities of vitreous silica tend to be higher than the values predicted by the Debye model (153).

Thermal Conductivity. Thermal conductivity data for transparent vitreous silica are listed in the following table (154):

Temperature, K	Thermal conductivity, W/(m·K)
100	0.674
200	1.126
300	1.37
400	1.51
500	1.62
600	1.74

Thermal conductivity at 25°C is 1.38 W/(m·K). The thermal conductivity of opaque silica is 20% lower than that of clear vitreous silica.

Phonon transport is the main conduction mechanism < 300°C. Compositional effects are significant because the mean free phonon path is limited by the random glass structure. Estimates of the mean free phonon path in vitreous silica, made using elastic wave velocity, heat capacity, and thermal conductivity data, generate a value of 520 pm, which is on the order of the dimensions of the SiO_4 tetrahedron (155). Radiative conduction mechanisms can be significant at higher temperatures.

Thermal diffusivity, a, is related to the thermal conductivity, k, through the following equation, where ρ is density and C_p is heat capacity. The value of a at 25°C is 9×10^{-3} cm^2/s (156).

$$a = k/(\rho C_p)$$

4.4. Mechanical Properties. *Moduli and Poisson's Ratio.* The Young's modulus of vitreous silica at 25°C is 73 GPa ($< 1.06 \times 10^7$ psi), the shear modulus is 31 GPa ($< 4.5 \times 10^6$ psi), and the Poisson's ratio is 0.17. Minor differences in values can arise owing to density variations. The elastic modulus decreases with increasing density and Poisson's ratio increases (26).

In contrast to the behavior of most glasses, the elastic moduli of vitreous silica increase with temperature, reaching a maximum at 1100–1200°C. The maximum is ~10% higher than the room temperature value (157). The high temperature values, however, are probably not accurate readings of the instantaneous moduli because viscous deformation is possible >1000°C.

Strength. The fracture strength of vitreous silica depends on its surface quality, which can be affected by thermal treatment and handling conditions. Microcracks, surface contamination, and crystallization can reduce the strength from the value of pristine vitreous silica by several orders of magnitude.

The theoretical estimates of the intrinsic strength of vitreous silica, based on structural considerations, range from 1.6 GPa (< 235,000 psi) to 2.3 GPa (< 338,000 psi) (158,159). Experimental values close to theoretical numbers have been obtained under carefully controlled conditions. These conditions involve fibers having undamaged surfaces and measurements made in vacuum at low temperatures. For example, tests run at −196°C detected strengths in excess of 1.3 GPa (191,000 psi) (160,161). Conversely, the room temperature strength of a flame-drawn fiber is decreased from ~4.7 GPa (< 690 psi) to 344 MPa (< 50,600 psi) by merely placing a finger on it (162).

The fracture strength of vitreous silica is also affected by environmental factors, eg, temperature and humidity. The temperature effect on the strength of flame-drawn fiber is shown in Figure 6. The strength of fused silica rods decreases in the presence of saturated vapors of alcohols, benzene, acetone, and water (163). The largest decrease is caused by water vapor, ie, almost 50% from a starting strength of 91 MPa (< 13,400 psi). Water vapor weakens vitreous silica by promoting crack growth. The critical fracture energy, Y_c, eg, is 4.3–4.4 J/m^2 (18–18.4 cal/m^2) in dry nitrogen gas at 27°C, and 3.7 J/m^2 (15.5 cal/m^2) in air at 40% rh (164,165).

Commercially available clear silicas typically have tensile strengths of 50–70 MPa (7,250–10,150 psi) and compressive strengths of 500–1900 MPa (72,500–275,500 psi). The opaque silicas have tensile strengths of 5–50 MPa (725–7250 psi) and compressive strengths of 190–300 MPa (27,550–43,500 psi) (166). Safety factors of 10–20-fold are usually employed when developing structural elements made of vitreous silica.

Fracture toughness is another way to characterize the strength of a material. It measures how well a material resists crack propagation and is expressed as the stress needed to enlarge a crack of a specific size. The room temperature fracture toughness of clear, vitreous silica is $\sim 0.75–0.80\ MPa \cdot m^{1/2}$ (87,167).

Hardness. The Knoop indentation hardness of vitreous silica is in the range of 473–593 kg/mm^2 and the diamond pyramidal (Vickers) hardness is in the range of 600–750 kg/mm^2 (168). The Vickers hardness for fused quartz decreases with increasing temperature but suddenly decreases at ~70°C. In addition, a small positive discontinuity occurs at 570°C, which may result from a memory of quartz structure (169). A maximum at 570°C is attributed to the presence of small amounts of quartz microcrystals (170). Scanning electron microscopic (sem) examination of the indentation area indicates that deformation is mainly from material compaction. There is little evidence of shear flow (171).

Ultrasonic Properties. Vitreous silica of high purity, such as the synthetic type, has an unusually low attenuation of high frequency ultrasonic waves. The loss, A, is a linear function of frequency, f, up to the 30–40-MHz region and can be expressed as $A = Bf$, where $B = 0.26\,dB{\cdot}MHz/m$ for shear waves and $0.16\,dB{\cdot}MHz/m$ for compressional waves (172).

The ultrasonic relaxation loss may involve a thermally activated structural relaxation associated with a shifting of bridging oxygen atoms between two equilibrium positions (173). The velocity, ù, of ultrasonic waves in an infinite medium is given by the following equation, where M is the appropriate elastic modulus, and density, d, is $2.20\,g/cm^3$.

$$\nu = (M/d)^{1/2}$$

At a shear modulus of 31.1 GPa (4.5×10^6 psi), vitreous silica has a plane–shear wave velocity of 3.76×10^5cm/s.

Shear velocity and acoustic absorption have been studied as a function of OH content and fictive temperature for four different vitreous silica samples (174). All showed a shear–velocity minimum at 80–100 K. The magnitudes of the minima are influenced by OH content and fictive temperature. The samples having the highest OH content and lowest fictive temperature display the lowest losses.

4.5. Electrical Properties. *Conductivity.* Pure vitreous silica is an excellent electrical insulator. The synthetic glasses can have bulk resistivities as high as $10^{18}\,\Omega{\cdot}cm$ at room temperature. Vitreous silica is an ionic conductor. Its large optical band gap (8.1 eV) precludes the formation of a significant concentration of electronic charge carriers (175). The main charge-carrying species are the monovalent cation impurities, especially sodium. Assuming an Arrhenius model, the activation energies of the conductivity at 350°C from sodium, lithium, and potassium ions are 85.9, 122.8, and 131.6 kJ/mol (20.5, 29.3, and 31.5 kcal/mol), respectively (176). The temperature dependence of the electrical conductivity, however, does not appear to follow strict Arrhenius behavior. The activation energy tends to decrease with increasing temperature. Part of the reason for this deviation may be glass electrode effects (177).

The surface conductivity of vitreous silica is also low compared to other silicate glasses. Because vitreous silica is not hydroscopic, water films containing exuded alkalies do not readily form on its surfaces. The surface conductivity, however, can increase significantly with increasing relative humidity. A change in the relative humidity from 20 to 80% produces a millionfold increase in the surface conductivity (178).

Dielectric Properties. Vitreous silica is also a very stable dielectric material. The dielectric constant is 3.8–4.0, depending on the grade of glass. The loss factor, usually < 0.00004, is the lowest available in glassy materials (87). The temperature and frequency dependences of both properties in a typical synthetic-grade vitreous silica are shown in Table 8. Lower purity silicas have slightly lower permittivities and higher loss factors. The loss factor is sensitive to impurities, especially the OH content of the glass (179). A discontinuity in loss

factor occurs near 570°C, the quartz transition temperature. This may reflect the presence of quartz-like regions in the glass.

The dielectric breakdown strength in vitreous silica depends on its impurity content, its surface texture, and the concentration of structural defects, eg, cord and bubbles. Good quality glasses have room temperature breakdown strength in the range of 200–400 kV/cm.

4.6. Optical Properties. The optical transmission of vitreous silica is influenced by dopants, impurities and the forming process. Ultrapure vitreous silica has the ability to transmit from the deep uv, through the visible, and into the near-ir spectral range. Transparency is also observed in the MHz to THz range of frequencies (180).

The uv cutoff or the absorption edge for pure vitreous silica is roughly 8.1 eV (174). This uv cutoff is influenced by the impurity level, the OH content of the glass and stoichiometry of the material. Vacuum uv reflectivity measurements coupled with spectroscopic ellipsometry measurements have recently yielded the most accurate determination of vuv optical properties of vitreous silica glass; these were compared to the same measurements performed on crystalline quartz (181). The two phases of silica (vitreous and crystalline) share the same structural building block, the SiO_4 tetrahedron, and so exhibit common interband transitions, at 10.4, 11.6, 14.03, and 17.10 eV. Interestingly, when comparisons are made between two cuts of crystalline quartz and vitreous silica there are other transitions that are unique to each material, occuring at different energies. The observed distinctions among the phases with respect to electronic spectra and optical properties are attributed to the intermediate and long-range order of each form of silica.

Alkali metal ions (Na, Li, K) degrade the uv performance by introducing nonbridging oxygen species, shifting the uv cutoff to longer wavelengths. Vitreous silica for optical applications in the uv then require purity in the ppb levels for alkali. Inclusion of transition metals into vitreous silica yields coloration from the ir (where optical abasorption is detrimental for optical waveguide performance) through the visible and into the uv (182). Ferric ions (Fe^{3+}), eg, cause absorption or result in network defects under reducing conditions. This contaminant at only a few ppm can be detected as an absorption at 230 nm and below (183).

A number of defects can be present in vitreous silica as a consequence of the forming conditions used to make the glass. These are reviewed in Ref. 184. An absorption band at 242 nm is characteristic of reduced vitreous silica manufactured by fusing crystalline quartz powders. This band is apparent in Type I and II silica, eg, ir Vitreosil, G.E.-124 fused quartz, Infrasil, Homosil, Herasil (Optosil), and most of the NSG quartz. The 242-nm absorption has been attributed to a number of defects that include Si^{2+} (185), Si^{3+} associated with Al^{3+} (186), and germanium-related oxygen-deficient centers (187,188).

The Si–O oscillation produces strong absorption bands at 8.83, 8.98, 12.41, and 21.37 μm. The fundamental vibration at 8.83 μm also has a strong overtone at 4.45 μm, ie, the practical infrared cutoff wavelength. Water incorporated in the silica structure gives rise to a very strong absorption at 2.73 μm, which is observed in Type I and II glass. A combination of the SiO_4 fundamental at 12.41 μm and the strong OH fundamental at 2.73 μm produces a peak at

2.22 μm observed in the high water content silicas (189). Hydroxyl content limits ir transmission in the telecommunications window at roughly 1.5 μm.

Vitreous silica transmission curves are shown in Figure 7. The hydroxyl concentration for each silica type is listed in Table 9. These curves represent only the general characteristics of the different silica types and should not be used for calculations of transmittance.

The spectral normal emissivity of Corning Code 7980 vitreous silica was computed from measurements of transmittance and reflectance at 25°C and is shown in Figure 8. The total normal emissivity of Code 7980 silica as a function of temperature from −200 to 1400°C is shown in Figure 9.

The index of refraction of synthetic vitreous silica at 20°C has been fitted to a three-term Sellmeier dispersion equation for wavelengths from 0.2139 to 3.7067 μm (192), where n is the refractive index and λ is the corresponding wavelength in micrometers.

$$n_D^2 - 1 = \frac{0.6961663\,\lambda^2}{\lambda^2 - (0.0684043)^2} + \frac{0.4079426\,\lambda^2}{\lambda^2 - (0.1162414)^2} + \frac{0.8974794\,\lambda^2}{\lambda^2 - (9.896161)^2}$$

The computed refractive index at 20°C is 1.534307 at 0.213856 μm, 1.508398 at 0.248272 μm, 1.474539 at 0.365015 μm, 1.45637 at 0.65627 μm, and 1.39936 at 3.7067 μm. Using suspect data removed from the computed index, the predicted index fit with an average deviation of 4.3×10^{-6} over the wavelength range of 0.21–2.32 μm (193). The Abbe constant, which describes the reciprocal of the dispersive power, is 67.8. Refractive index also changes with temperature. The average values of $\Delta n_D/\Delta T$ at 25°C are shown in Figure 10. The $\Delta n/\Delta T$ values as a function of temperature from −200 to 40°C are shown in Figure 11 for vitreous silica at 587.6 nm. The stress optical coefficient, sometimes referred to as stress birefringence constant, is 3.45 nm/(cm·Pa). Vitreous silica refractive index is affected by the chlorine, fluorine, and hydroxyl concentration. An increase in the hydroxyl concentration of 1 ppm results in a decrease in refractive index of 1×10^{-7} (194). Fluorine additions lower the refractive index; in the visible, it is found that addition of 1 wt% F lowers the index by 0.3% (195). Another factor that can influence the refractive index is the thermal history of the glass (196,197).

4.7. Radiation Effects. Because vitreous silica possesses desirable physical and optical characteristics (low thermal expansion and high transparency over a wide wavelength range, eg) it is used for a wide variety of applications where it is subjected to all types of radiation. There are numerous reports of the behavior of vitreous silica under exposure to particle radiation, electron beams, X-rays, protons and photons. As a consequence of exposure to irradiation, however, vitreous silica can undergo changes in volume and exhibit formation of optical absorption centers (color center formation).

Irradiation by fast neutrons causes a densification of vitreous silica that reaches a maximum value of 2.26 g/cm^3, ie, an increase of ∼ 3%, after a dose of 1×10^{20} neutrons/cm^2. Doses of up to 2×10^{20}n/cm^2 do not further affect this density value (199). Quartz, tridymite, and cristobalite attain the same density after heavy neutron irradiation, which means a density decrease of 14.7% for quartz

and 0.26% for cristobalite (200). The resulting glass-like material is the same in each case, and shows no X-ray diffraction pattern, but has identical density, thermal expansion (201), and elastic properties (202). Other properties are also affected, ie, the heat capacity is lower than that of vitreous silica (203), the thermal conductivity increases by a factor of 2 (204), and the refractive index, n_D, increases to 1.4690 (205).

Irradiation by both X- and γ-rays produces absorption centers in vitreous silica, although structural damage is reported to be negligible. These absorption centers show up primarily in the visible and uv spectral regions. Little change is seen in the infrared region; a Raman line at 606 cm^{-1} has been ascribed to nonbridging oxygen defects (206). The types and number of absorption centers produced depend on the purity of the vitreous silica and the total radiation dosage received. The rate of coloration of high purity vitreous silica, ie, very low concentration of metallic impurities, eg, Type III silica, is very slow, and doses of $\geq$10 Gy (10^7 rad) are required to obtain appreciable absorption. For comparable absorption intensities in less-pure material, ie, silica Types I and II, radiation approximately two orders of magnitude lower is required (207). Extensive research has been conducted in the field of radiation-induced absorption centers in vitreous silica. Excellent reviews, including a thorough compilation of all absorption centers studied, are available (184,208–210). Only the principal centers and their probable causes are discussed herein.

A typical absorption curve for vitreous silica containing metallic impurities after X-ray irradiation is shown in Figure 12. As shown, the primary absorption centers are at 550, 300, and between 220 and 215 nm. The 550-nm band results from a center consisting of an interstitial alkali cation associated with a network substituent of lower valency than silicon, eg, aluminum (208). Only alkalies contribute to the coloration at 550 nm. Lithium is more effective than sodium, and sodium more effective than potassium. The intensity of the band is determined by the component that is present in lower concentration. The presence of hydrogen does not appear to contribute to the 550-nm color-center production (211).

The absorption band at 300 nm may also be associated with alkali ions, possibly the result of a trapped electron stabilized by an alkali ion. The band shifts to longer wavelengths when heavier alkali ions are present, and growth rates for the band show a definite dependence on the type of alkali (208,211).

The 215-nm band is the well-studied E' center. This band can be produced in all vitreous silicas by long-term X-ray irradiation (213). The E' center, which may also be observed in irradiated α-quartz, has been structurally elucidated to be a pyramidal SiO_3 unit having an unpaired electron in the dangling sp^3 orbital of Si. This center will be discussed again with respect to uv applications of vitreous silica.

A typical absorption curve obtained for a metal-free vitreous silica after a large dose of γ-rays is shown in Figure 13. The main band is at 215 nm; three smaller bands occur at 230, 260, and 280 nm. The 230-nm band may result from an electron trapped at a silicon atom having an incomplete oxygen bond (208).

Excimer lasers (qv) generate pulsed light having very high instantaneous peak powers. These lasers operate in the uv and deep ultraviolet (duv) at 308, 248, and 193 nm, and have been found to cause laser-induced optical changes

(color center formation) and volume changes in vitreous silica. The subband gap light generated by excimer lasers excites electrons into the valance band by a multiphoton process. Transmission measurements made as a function of intensity show that the two-photon absorption (TPA) coefficient is $\sim(1.9–3.0)\times10^{-10}$ cm/W at 193 nm and 4.5×10^{-11}cm/W at 248 nm (215).

Color centers in the uv that are of interest are the E' center and the nonbridging oxygen-hole center (NBOHC), which arise schematically by the process shown:

$$(O)_3{-}Si{-}O{-}Si{-}(O)_3 + \text{light} \rightarrow \underset{E'}{(O)_3{-}Si^{\bullet}} + \underset{NBOHC}{(O)_3{-}Si{-}O^{\bullet}}$$

For applications that use silica as the lens material for 193-nm related applications (specifically the microlithography industry) the formation of the E' center discussed previously is of critical importance. This defect is centered at 215 nm and has a half-width of 0.8 eV (184) decreasing transmission at the use wavelength. Schemes to mitigate E' color center formation involve the use of H_2 (which reacts with the E' to yield the essentially nonabsorbing SiH) (216,217). Similarly, for applications using a 248-nm light source, the light-induced formation of the NBOHC is important; its absorption is at 260 nm with a half-width of 1.05 eV (184), yielding absorption at the use wavelength. One practical upshot of absorption at the use wavelength for imaging applications is the effects of lens heating and ultimately image disstortion.

Volume changes in excimer-irradiated vitreous silica have also been studied (133,135,136,218,219). In comparison to exposures to neutrons, eg, where density increases in the percent range are noted, exposure to uv irradiation results in changes in the parts per million level. These changes are typically deduced from interferometric measurements of the change in (nL), the optical pathlength (where n = refractive index, L = physical pathlength), and from interpretation of a stress-induced birefringence measurement (133). The behavior of the uv-induced volume changes in vitreous silica is quite complicated, depending on the glass composition, the incident fluence and number of pulses. With 193-nm exposure, high fluence exposures (>5 mJ/cm^2) yield only increased density, regardless of OH and H_2 content. At lower fluences (<1 mJ/cm^2) the density change can be monotonically increasing with pulses or decreasing with pulses (expanding). Densification followed by expansion at higher pulse count has also been observed (135). Thermal reaction of various silicas has also yielded lower density glass, the interpretation relying on the formation of SiOH and SiH, leading to lower density (137).

5. Economic Aspects

The market for fused silica started in 1906 with the sale of silica muffles and pipes. That same year resulted in the incorporation of the Thermal Syndicate Ltd. Since that time, worldwide sale of vitreous silica material and fabricated products has continued to grow. The sales of vitreous silica ingots, tubes, rods,

plates, fabricated products, photomask blanks, crucibles, and optics was estimated to be between $800 million to $1.3 billion in 2000. These figures do not, however, take into account the optical waveguide market based on fused silica technology.

In constant dollars, many items have decreased in cost over the past 20 years because of improved manufacturing methods, new raw material sources, and higher production volumes. However, many new products have been developed since the mid-1980s, eg, optics for photolithography and excimer lasers, whereas others have been practically displaced by newer materials or technologies. The illumination and projection optics for optical lithography are a critical market for synthetic fused silica. The stepper and scanner technology used for the production of integrated circuits (qv) is shifting to shorter wavelength light sources in order to improve resolution. These deep uv wavelengths require synthetic fused silica optics. The annual growth rate for the projection optics is estimated at between 9 and 12%/year, averaged over a few years for stepper–scanner. In addition, integrated circuit manufacturing is increasing silicon wafer sizes from 200 to 300 mm in diameter, thereby creating a significant increase in demand for high purity fused silica tubing for diffusion furnaces, and silicon wafer furniture. The principal U.S. and foreign manufacturers of vitreous silica are listed in Table 10.

6. Uses

6.1. Chemical Applications. Because of its excellent chemical durability, high purity, thermal shock resistance, and usefulness at high temperature, vitreous silica has a wide range of applications in chemical analysis and preparations. Tubing, rods, crucibles, dishes, boats, and other containers and special apparatus are available in both transparent and nontransparent varieties (120,141,142,220). Because of its inertness, vitreous silica is used as a chromatographic substrate in the form of microparticles, capillary tubing, and open columns for high resolution gas chromatography (see ANALYTICAL METHODS; CHROMATOGRAPHY) (221).

6.2. Thermal Applications. The protection of precious-metal thermocouples in high temperature pyrometry is an important application of vitreous silica. Although satin tubing is usually employed, transparent tubes are superior for protecting couples when used in a reducing atmosphere (222).

Vitreous silica is used for gas- or electrically heated devices in various shapes, eg, as a tube or muffle because of its electrical resistivity, impermeability, and low expansion. In its simplest form, an electric-resistance furnace consists of a vitreous silica tube or pipe on which the resistance element is wound (see FURNACES, ELECTRIC INTRODUCTION). Because of its indifference to temperature gradients, a tubular furnace of vitreous silica may be made to operate at different temperatures at various portions of the tube, either by arrangement of the heating elements or by cooling sections of the tube with water. Vitreous silica pipes may be employed in vacuum induction and gas-fired furnaces (see VACUUM TECHNOLOGY) (223).

Radiant heaters employing resistance wire encased in vitreous silica tubes have the capability to modify the emitted radiation and furnish a higher proportion of shorter (1–2 μm) wavelengths that constitute the desirable radiations. Immersion heaters for use with acid solutions are of similar construction. An overhead heating unit consisting of a resistance wire sealed inside a vitreous silica container permits acid liquids to be concentrated or evaporated without ebullition or spattering. High efficiency radiators ~200-cm long have been developed for power requirements up to 6 kW. These are used as energy sources in heat exchangers (see HEAT-EXCHANGE TECHNOLOGY), high duty enamel drying equipment, polymerization processes, and copying devices (223).

Insulation having high thermal endurance has been made from vitreous silica fibers (see ABLATIVE MATERIALS). Such material forms the basis for the 30,000 insulating tiles, 125-mm thick, that protect the aluminum skin of the space shuttle. The tiles add a minimum of weight because the density of the insulation is only 144 kg/m^3 (9 lb/ft^3), similar to balsa wood.

Optical Applications. Vitreous silica is ideal for many optical applications because of its excellent uv transmission, resistance to radiation darkening, optical polishing properties, and physical and chemical stability. It is used for prisms, lenses, cells, windows, and other optical components where uv transmission is critical. Cuvettes used in scatter and spectrophotometer cells are manufactured from fused silica and fused quartz because of the transmissive properties and high purity (224).

The development of high power laser systems at shorter uv wavelengths requires the transmissive and optical properties of fused silica. These high power lasers are utilized for commercial energy research and military applications. Excimer lasers are utilized in photoablation, photolithography, material processing, and medical applications. The optical beam delivery systems for these excimers can utilize fused silica lenses or optical fibers (225,226), as well as fluoride-based optics, eg, CaF_2 and MgF_2.

All higher energy laser systems throughout the world utilize a significant amount of high quality fused silica. Inertial confinement research laser systems, such as the Lawrence Livermore National Laboratory (LLNL) NIF (National Ignition Facility) laser that operates at 366 nm (frequency tripled Nd–YAG laser), require fused silica for the transport and cavity spatial filter lendes, Pockel cell windows, vacuum windows, final focal lens and the debris shield (227). Inertia confinement fusion research is also underway using KrF (248-nm) laser systems, eg, the Los Alamos Aurora and Naval Research Laboratory NIKE. These utilize a fused silica (Corning Code 7980).

6.3. Mechanical Applications. The volume of vitreous silica used for fibers is a very small part of the total consumption. However, some interesting and significant applications have been developed in the laboratory, particularly in the area of measurements.

The sorption balance employs 15 small vitreous silica springs enclosed in glass tubes (228). The fiber is 2 mm in diameter and the coils 1.25 cm in diameter and 5.99 cm long (see WEIGHING AND PROPORTIONING). A platinum bucket, which weighs 202 mg, contains up to 0.5-g charcoal; the balance can be read to 0.2 mg. The sorption of gases is determined over a wide range of temperatures and pressures. This type of balance has been used for density determinations,

measurements of heat loss and evaporation, study of chemical reactions between gas and solid phases, and weight determination of wet tissues of plant and animal origin. The advantages of vitreous silica are its resistance to corrosion, ease of cleaning and sterilization in an enclosed tube, and absence of damping from internal friction.

Because of its low and regular thermal expansion, vitreous silica is employed in apparatus used to measure the thermal expansion of solids. A detailed account of the different methods used for this purpose has been published (229). The most common form of dilatometer utilizes a vitreous silica tube closed at the bottom and containing the test sample. A movable rod of vitreous silica, resting on the sample, actuates a dial indicator resting on the top of the rod. The assembly containing the sample is placed in a furnace, bath, or cooling chamber to attain the desired temperature.

6.4. Lighting. An important application of clear fused quartz is as envelop material for mercury vapor lamps (230). In addition to resistance to deformation at operating temperatures and pressures, fused quartz offers uv transmission to permit color correction. Color is corrected by coating the inside of the outer envelope of the mercury vapor lamp with phosphor. Ultraviolet light from the arc passes through the fused quartz envelope and excites the phosphor, producing a color nearer the red end of the spectrum (231). A more recent improvement is the incorporation of metal halides in the lamp (232,233).

Incandescent tungsten–halogen (F, Br, I) cycle lamps first became available in 1959 for general use. In this lamp, tungsten evaporating from the filament deposits on the envelope wall where it reacts with halogen vapor to form a volatile halide. The tungsten halide diffuses back to the filament where it dissociates to halogen vapor and tungsten. This permits a higher temperature operation, which affords higher efficiency and longer life than the conventional incandescent lamp. The wall temperature must be at least 250°C and, if possible, $\sim$600°C. Fused quartz has been essential for this development because it is one of the few readily available transparent materials that can be used in lamp envelopes. Improvements include the internal deposition of a barrier, eg, aluminum fluoride or aluminosilicate (234,235), and reflective layers, eg, titanium silicate or zirconia (236,237). These protect the silica glass from vapor attack, slow the diffusion of deactivating impurities, and reflect heat onto the filament while transmitting visible light. These lamps are used in the illumination of airfields, sports arenas, buildings, streets, parking lots, and automobiles. They are also used in slide and film projectors and specialized optical instruments (238,239).

6.5. Electronic Applications. In electronic systems, such as radar and computers, signal delay is sometimes necessary. A transducer converts electrical signals to ultrasonic elastic waves, which pass through a connecting medium to another transducer, where the waves are reconverted to electrical signals. Vitreous silica is an ideal connecting medium because it has excellent physical stability and low ultrasonic transmission losses. It transmits an ultrasonic signal almost 100,000 times more slowly than an electric signal in a wire. The vitreous silica delay line is in the form of a flat polyhedral plate. The facets of the edges of this plate are ground to a predetermined angle with great precision. The transducer is fastened to one of these facets. The plates may be designed for path

lengths of 4 cm to nearly 12 m, giving delay times for shear waves of 10–3000 μs (240).

By far the most significant electronic application, and perhaps the highest volume application for vitreous silica, is in semiconductors (qv). This association began with silicon wafer technology, where vitreous silica was the principal high purity material for crucibles for silicon crystal growth. Both opaque sintered and transparent vitreous silica from tubing or boules are used. Crucible sizes have been increasing in response to the demand for ever-larger silicon wafers.

Vitreous silica tubes are used for the subsequent high temperature diffusion, doping, and epitaxial growth treatments performed on wafers destined for large-scale integrated circuits. Once again, the high purity of certain grades of vitreous silica, along with its high thermal endurance, make it the material of choice for diffusion tubes, wafer holders, boats, and associated hardware. Quartz manufacturers continue to push for higher purity, ie, alkali content in tubing approaching <1 ppm. The thermal endurance of the tubes may be prolonged by causing some surface crystallization; the increased rigidity prevents sagging (141). Diffusion-resistant barrier coatings have also been used (241,242). In addition to silicon wafers, many other high temperature, high purity solid-state reactions are performed in vitreous silica vessels, including crystal growth, zone refining, and the preparation of gallium and indium arsenides, as well as germanium and silicon optical materials.

Thin films (qv) of vitreous silica have been used extensively in semiconductor technology. These serve as insulating layers between conductor stripes and a semiconductor surface in integrated circuits, and as a surface passivation material in planar diodes, transistors, and injection lasers. They are also used for diffusion masking, as etchant surfaces, and for encapsulation and protection of completed electronic devices. Thin films serve an important function in multilayer conductor insulation technology where a variety of conducting paths are deposited in overlay patterns and insulating layers are required for separation.

Thin vitreous silica films are usually formed by vapor deposition or r-f sputtering (see THIN FILMS, FILM-DEPOSITION TECHNIQUES). Vapor deposition is generally effected by the pyrolytic decomposition of tetraethoxysilane or another alkoxysilane. Silica has been most extensively used in r-f sputtering of dielectric films, which are of very high quality.

Large-scale and very large-scale integration (VLSI) of electronic circuits requires the photoreduction of complex conductor and insulator patterns, which are reproduced on semiconductor devices by various photoresist processes. Vitreous silica is frequently used for the photomask substrate, ie, the transparent substrate for the image mask that contains the basis for conduction or insulator patterns. Because of the extremely high dimensional tolerances of VLSI, vitreous silica is a natural choice for the substrate. Its uv transmission properties allow fast exposure of the photoresists, and its very low thermal expansion prevents pattern distortions owing to temperature gradients encountered during processing. Perfectly flat and inclusion-free material is required (243). Another application for fused silica in the semiconductor field is as optical elements in microlithographic systems. In order to obtain smaller features on computer chips, ie, increasing the memory capacity, photolithographic stepper and scanner systems are moving to shorter wavelengths. Vitreous silica is used to make the

excimer-based deep uv (248 and 193 nm) lithographic lens systems because of its superior uv transmission and radiation resistance characteristics. These lens systems are used to manufacture 256-Mb dynamic random-access memory computer chips(DRAM) (226) and increasingly higher density NAND and NOR flash memory chips, whose growth rate is currently (2006) > 30%/year. The refinement of silica properties for use at 193nm (particularly radiation resistance) is particularly important because 193-nm technology is being optimized further than previously thought possible. These systems are now being extended to manufacture circuit dimensions of < 100 nm; this size was once intended to be manufactured using 157-nm lithography or other future technologies. In addition, titanium-doped silica (eg, Corning Incorporated ULE) is being explored for its use in extreme uv (13nm) lithography. Mirrors made from materials such as this offer the lultralow thermal expansion required for producing features in the 20-nm range.

6.6. Space and Astronomy. Vitreous silica is used in several space-based applications because of static fatigue (slow crack growth), thermal stability, and radiation resistance. Every U.S. space vehicle having service personnel, including Mercury, Gemini, Apollo, and space shuttle vehicles, has been equipped with windows made of high optical-quality vitreous silica (Corning Code 7940 or 7980) in order to have the clarity needed for visual, photographic, and television-based observations. The space shuttle utilizes triple-layer windows that have outer and central panes of vitreous silica with a tempered aluminosilicate inner pane. The outer pane is thinner for thermal endurance, whereas the two inner panes are thicker to supply strength (244).

The ability of vitreous silica to withstand dimensional changes with changing temperature has made it ideal for mirror blanks of telescopes (245–247). Vitreous silica is used in both space- and ground-based mirror applications because of the thermal stability and the ability to polish to ultrasmooth surface. The mirrors for space-based applications are fabricated by fusion-sealing struts into a honeycomb structure of vitreous silica, which is then fused or bonded with expansion-matching materials to top (face plate) and bottom (backer) plates. Weight reductions of up to 93%, relative to the weight of an equivalent-sized solid glass blank, can be achieved using these sandwich structures.

An ultralow expansion (ULE) vitreous silica (ULE-Corning Code 7972) can be manufactured by doping the silica with a 7.5% titanium dioxide (148,244). The sonic velocity and coefficient of thermal expansion (CTE) are directly related to the titanium concentration. This material was used to manufacture the 2.4 m dia lightweight mirror blank for the Hubble telescope and the 8.3-m mirror blank for the ground-based Japanese National Large Telescope (JNLT). The JNLT piece, the largest mirror blank in the world, was manufactured by hex-sealing titanium-doped vitreous silica pieces into a solid glass mirror weighing >30 t (248).

Space-based solar cells are covered with a very thin layer of vitreous silica to protect against the damaging environment of space such as atomic oxygen, micrometeorites, and radiation effects. Because the silica is transparent to damaging uv radiation, it is normally coated with a uv-reflective thin film (see SOLAR ENERGY).

The Topex oceanographic satellite used a laser-based retroreflector array for positioning. The retroreflectors were manufactured from Corning Code 7958 fused silica, a sol–gel-derived low water vitreous silica material (249).

6.7. Optical Fibers. Pure and doped fused silica fibers have replaced copper lines in the telecommunication area. Fused silica fibers are used in laser surgery, optical sensor application, and laser welding (see SENSORS). Optical-fiber-tethered weapons, eg, fiber-optics-guided (FOG) missiles are another potential application for fused silica (250,251). Silica glass has also been used to fabricate microstructured air-core photonic band gap fibers (252). These fibers consist of an air core surrounded by a periodic lattice of air holes in glass. Light guidance in these fibers is based on the principle of interference to reflect radiation. The fibers can be made in long lengths, starting with a "stack-and-draw" process (253,254). In this process, a preform of silica capillaries is stacked into the desired lattice. Subsequent drawing processes reduce the pre-form to fiber dimensions (typically for telecommunications applications the final fiber diameter is 120 μ). The lattice spacing of the air holes is on the order of 3–5 μ for the telecommunications applications; glass thickness between the air holes is on the order of hundreds of nanometers. Much of the success of silica in these applications can be related to its wide working range. (see FIBER OPTICS).

6.8. Other Uses. Vitreous silica also has applications in the form of powders, fibers, wool, and chips (255). The powder may be used as an inert filler or as a coating material in the investment-casting industry for the lost-wax process. Chips are used as an inert substrate in certain chemical process applications. Vitreous silica wool or fiber is an excellent insulation or packing material. Complex shapes rendered in extruded or sintered vitreous silica are used to produce precisely shaped holes, tunnels, cavities, and passages in investment-cast metal parts (see also REFRACTORIES). The vitreous silica shapes are chemically compatible with most alloys and dimensionally stable at casting temperatures. They give smooth internal surfaces to the cast pieces. The cooled casting is subsequently treated in hot caustic solutions to remove the silica core. Sandblasting may also be used. Internal features such as long holes and cooling passages for turbine rotors, which would be impossible to fabricate by drilling or machining, are obtained routinely (256).

Antireflective (AR) coatings are required on optics to reduce the reflective surface losses. Vitreous silica coatings in the form of porous or multilayer films are used extensively in this application. Antireflective coatings have been developed that employ colloidal fused silica sol–gel particles made from organometallic materials (257).

BIBLIOGRAPHY

"Vitreous Silica" under "Silica and Silicates" in *ECT* 1st ed., Vol. 12, pp. 335–344, by W. Winship, The Thermal Syndicate Ltd.; "Silica, Vitreous" in *ECT* 2nd ed., Vol. 18, pp. 73–105, by W. H. Dumbaugh and P. C. Schultz, Corning Class Works; in *ECT* 3rd ed., Vol. 20, pp. 782–817, by P. Danielson, Corning Glass Works; in *ECT* 4th ed., Vol. 21, pp. 1032–1075, by D. R. Sempolinski and P. M. Schermerhorn, Corning, Inc.; "Silica, Vitreous

Silica" in *ECT* (online), posting date: December 4, 2000, by D. R. Sempolinski and P. M. Schermerhorn, Corning, Inc.

CITED REFERENCES?

1. F. E. Wagstaff, *J. Am. Cer. Soc.* **52**, 650 (1969).
2. R. B. Sosman, *The Phases of Silica*, Rutgers University Press, New Brunswick, N.J., 1965, pp. 164–165.
3. B. J. Skinner and J. J. Fahey, *J. Geophys. Res.* **68**(19), 5595 (1963).
4. Ref. 2, pp. 148–150.
5. J. S. Laufer, *J. Opt. Soc. Am.* **55**, 458 (1965).
6. G. Hetherington, *J. Br. Ceram. Soc.* **3**(4), 595 (1966).
7. I. Fanderlik, ed., *Silica Glass and its Application*, Elsevier Science Publishers, New York, 1991, pp. 165–166.
8. G. Hetherington, K. H. Jack, and J. C. Kennedy, *Phys. Chem. Glasses* **5**(5), 130 (1964).
9. D. N. Casey, G. Hetherington, J. A. Winterburn, and B. Yates, *Phys. Chem. Glasses* **17**(3), 77 (1976).
10. L. L. Hench, S. H. Wang, and J. L. Nogues, *Multifunctional Materials*, SPIE Vol. 878, Society of Photooptical Engineers, Bellingham, Wash., 1988, pp. 76–85.
11. D. Torikai and co-workers, *J. Non-Cryst. Solids* **179**, 328 (1994).
12. R. L. Mozzi and B. E. Warren, *J. Appl. Crystallogr.* **2**, 164 (1969).
13. E. Lorch, *J. Phys. C* **2**, 229 (1969).
14. A. C. Wright, *J. Non-Cryst. Solids* **179**, 84 (1994).
15. D. I. Grimley, A. C. Wright, and R. N. Sinclair, *J. Non-Cryst. Solids* **119**, 49 (1990).
16. D. L. Price and J. M. Carpenter, *J. Non-Cryst. Solids* **92**, 153 (1987).
17. J. R. G. de Silva, D. G. Pinatti, C. E. Anderson, and M. L. Rudee, *Philos. Mag.* **31**, 713 (1975).
18. V. E. Sokol'skii, V. A. Shovskii, V. P. Kazimirov, and G. I. Batalin, *Fiz. Khim. Stekla* **6**(5), 517 (1980).
19. R. J. Bell and P. Dean, *Philos. Mag.* **25**, 1381 (1972).
20. A. E. Geissberger and F. L. Galeener, *Phys. Rev. B* **28**(6), 3266 (1983).
21. J. C. Mikkelsen and F. L. Galeener, *J. Non-Cryst. Solids* **37**, 71 (1980).
22. E. A. Porai-Koshits, *J. Non-Cryst. Solids* **73**, 79 (1985).
23. J. C. Phillips, *Phys. Rev. B* **32**, 5350 (1985); **33**, 4443 (1986).
24. D. L. Griscom, *J. Non-Cryst. Solids* **73**, 51 (1985).
25. F. L. Galeener, in R. A. Weeks and D. L. Kinser, eds., *Effects of Modes of Formation on the Structure of Glasses*, Trans Tech Publications Ltd., Brookfield, Vt., 1987, pp. 305–314.
26. R. Bruckner, *J. Non-Cryst. Solids* **5**, 123 (1970); **5**, 177 (1971).
27. D. L. Griscom, *J. Cer. Soc.* (*Jpn.*) **99**(10), 923 (1991).
28. G. C. Escher, *Excimer Beam Application*, SPIE Vol. 998, Society of Photooptical Engineers, Bellingham, Wash., 1988, pp. 30–37.
29. J. E. Shelby, *J. Non-Cryst. Solids* **179**, 138 (1994).
30. K. Awazu and co-workers, *J. Appl. Phys.* **69**(4), 1849 (1991).
31. T. E. Tsai, D. L. Griscom, and E. J. Friebele, *Phys. Rev. B* **38**(3), 2140 (1988).
32. D. L. Griscom, M. Stapelbroek, and E. J. Friebele, *J. Chem. Phys.* **78**(4), 1638 (1983).
33. Ref. 2, pp. 96–97.
34. C. R. Gaudin, *Acad. Sci.* (*Paris*) **8**, 678 (1839).
35. Ref. 2, p. 809.

36. W. A. Shenstone, *Nature* (*London*) **61**(1588), 540 (1900).
37. W. A. Shenstone and H. G. Lacell, *Nature* (*London*) **62**(1592), 20 (1900).
38. W. C. Heraeus, *Z. Electrochem.* **8**, 861 (1902); **9**, 847 (1903).
39. U.S. Pat. 2,268,589 (1942), J. A. Heany (to Heany Industrial Ceramics Corp.).
40. U.S. Pat. 2,272,342 (1942), J. F. Hyde (to Corning Glass Works).
41. Brit. Pat. 10,670 (1904), J. F. Bottomley, R. S. Hutton, and R. A. S. Paget.
42. Brit. Pat. 10,437 (1904), J. F. Bottomley and R. A. S. Paget.
43. U.S. Pat. 2,155,131 (Apr. 18, 1939), W. Hanlein (to Patent-Treuhand-Gesellschaft für Elektrische Glöhlampen GmbH).
44. U.S. Pat. 3,764,286 (Oct. 9, 1973), S. Antczak and co-workers (to General Electric Co.).
45. U.S. Pat. 2,904,713 (Sept. 15, 1959), W. H. Heraeus and H. Mohn (to Heraeus Quarzschmelze GmbH).
46. U.S. Pat. 3,128,166 (Apr. 7, 1964), H. Mohn (to Heraeus Quarzschmelze GmbH).
47. U.S. Pat. 2,270,718 (Jan. 20, 1942), F. Skaupy and G. Weissenberg.
48. U.S. Pat. 4,072,489 (Feb. 7, 1978), T. A. Loxley and co-workers (to Sherwood Refractories, Inc.).
49. U.S. Pat. 3,837,825 (Sept. 24, 1974), T. A. Loxley and co-workers (to Sherwood Refractories, Inc.).
50. U.S. Pat. 3,775,077 (Nov. 27, 1973), C. A. Nicastro and co-workers (to Corning Glass Works).
51. Fr. Demande 2,399,978 (1978), T. Izawa, T. Kuwabara, and Y. Masuda (to Nippon Tel.).
52. K. Nassau and J. Shiever, *Am. Cer. Soc. Bull.* **54**, 1004 (1975).
53. A. Audsley and R. K. Bayliss, *J. Appl. Chem.* **19**, 33 (1969).
54. A. D. Pinnow and W. F. Dabby, *Mater. Res. Bull.* **10**(12), 1263 (1975).
55. U.S. Pat. 5,043,002 (Aug. 27, 1991), M. S. Dobbins and R. E. McLay (to Corning Inc.).
56. Brit. Pat. 2,245,553 (Aug. 8, 1992), I. G. Sayce, Alan Smithson, and P. J. Wells (to Thermal Syndicate Ltd.).
57. G. D. Ulrich and J. W. Riehl, *J. Colloid Inter. Sci.* **87**(1), 257 (1982).
58. B. S. Aronson, D. R. Powers, and R. G. Sommer, *Proceedings of Topical Meeting on Optical Fibre Communication*, Washington, D.C., 1979.
59. S. Sudo and co-workers, *Electron. Lett.* **14**, 534 (1978).
60. K. J. Beales and C. R. Day, *Phys. Chem. Glasses* **21**(1), 5 (1980).
61. P. C. Schultz, *Appl. Opt.* **18**(21), 3684 (1979).
62. E. M. Dianov and co-workers, *Sov. Lightwave Comm.* **2**, 79 (1992).
63. S. Kobayashi and co-workers, *Appl. Opt.* **14**(12), 2817 (1975).
64. I. Matsuyama and co-workers, *Am. Cer. Soc. Bull.* **63**(11), 1408 (1984).
65. J. Opitz, *Glastech. Ber.* **60**(4), 133 (1987).
66. L. L. Hench, *Cer. Int.* **17**, 209 (1991).
67. L. C. Klein, *Glass Ind.* **62**(1), 14 (Jan. 1981).
68. R. Clasen, *Glastech. Ber.* **60**(4), 125 (1987).
69. G. W. Scherer and J. C. Luong, *J. Non-Cryst. Solids* **63**, 163 (1984).
70. U.S. Pat. 4,059,658 (Nov. 22, 1977), R. D. Shoup and W. J. Wein (to Corning Glass Works).
71. K. Susa and co-workers, *J. Non-Cryst. Solids* **79**, 165 (1986).
72. E. M. Rabinovich and co-workers, *J. Non-Cryst. Solids* **82**, 42 (1986).
73. S. Wang and co-workers, *Sol–Gel Optics II*, SPIE Vol. 1758, Society of Photooptical Engineers, Bellingham, Wash., 1992, pp. 113–124.
74. U.S. Pat. 4,789,389 (Dec. 6, 1988), P. M. Schermerhorn, M. P. Teter, and R. V. Vandewoestine (to Corning Glass Works).

75. Personal communication, F. Foster, Applied Laser Systems, Inc., Santa Clara, Calif., 1981.
76. W. G. Houskeeper, *J. Am. Inst. Electr. Eng.* **42**, 954 (1923).
77. O. L. Anderson and C. J. Dienes, in V. D. Frechette, ed., *Non-Crystalline Solids*, John Wiley & Sons, Inc., New York, 1960, pp. 449–486.
78. J. Arndt, R. A. B. Devine, and A. G. Revesz, *J. Non-Cryst. Solids* **131–133**, 1206 (1991).
79. F. M. Ernsberger, in D. R. Uhlmann and N. J. Kreidl, eds., *Elasticity and Strength in Glass*, Vol. 5, Academic Press, Inc., New York, 1980, pp. 9–12.
80. F. P. Mallinder and B. A. Procter, *Phys. Chem. Glasses* **5**, 91 (1964).
81. C. W. Morey, *The Properties of Glass*, Reinhold Publishing Corp., New York, 1954, pp. 319–320.
82. C. L. Babcock, *Silicate Glass Technology Methods*, John Wiley & Sons, Inc., New York, 1977, pp. 56–62.
83. M. R. Vukcevich, *J. Non-Cryst. Solids* **11**, 25 (1972).
84. R. K. Iler, in E. Matijevic, ed., *Surface and Colloid Science*, Vol. 6, Wiley-Interscience, New York, 1973.
85. W. Stober, *Kolloid-Z.* **147**, 131 (1956).
86. R. Moseback, *J. Geol.* **65**, 347 (1957).
87. *Fused Silica Code 7940 Data Sheet*, Corning Glass Works, Corning, N.Y., 1992.
88. J. J. Miller and D. L. Eppink, *Leaching of Preformed Ceramic Cores*, Sherwood Refractories, Inc., Cleveland, Ohio, 1977.
89. Y. Oka and M. Tomozawa, *J. Non-Cryst. Solids* **42**, 535 (1980).
90. R. Kleinteich, *Quarzglas Quarzgut Inst. Tech.* **9**, 334; **10**, 365; **11**, 409; **12**, 449 (1961).
91. Ref. 7, p. 201.
92. D. T. Liang and D. W. Readey, *J. Am. Cer. Soc.* **70**(8), 570 (1987).
93. Ref. 2, p. 146.
94. C. A. Elyard and H. Rawson, *Proceedings of the 6th International Congress on Glass*, Washington, D.C., 1962, pp. 270–286.
95. *Vitreosil*, Thermal American Fused Quartz Co., Montville, N.J., 1966.
96. G. H. A. M. VanderSteen, Ph.D. dissertation, Eindhoven, The Netherlands, 1976, pp. 64–70.
97. J. E. Shelby, *J. Non-Cryst. Solids* **179**, 138 (1994).
98. D. W. Green and R. H. Perry, eds., *Perry's Chemical Engineer's Handbook*, 6th ed., McGraw-Hill Book Co., Inc., New York, 1984, pp. 3–49.
99. A. deRudney, *Vacuum* **1**, 204 (1951).
100. W. D. Kingery, H. K. Bowen, and D. R. Uhlmann, *Introduction to Ceramics*, John Wiley & Sons, Inc., New York, 1976, p. 87.
101. N. C. Ainslie, C. R. Morelock, and D. Turnbull, *Proceedings of Symposium on Nucleation and Crystallization in Glasses and Melts*, Toronto, Canada, 1961, pp. 97–107.
102. H. Rawson, *Inorganic Glass-Forming Systems*, Academic Press, Inc., New York, 1967, pp. 48–61.
103. P. P. Bihuniak, *Comm. Am. Cer. Soc.* **66**(10), C188 (Oct. 1983).
104. F. E. Wagstaff, S. D. Brown, and I. B. Cutler, *Phys. Chem. Glasses* **5**(3), 76 (1964).
105. A. G. Boganov, V. S. Rudenko, and C. L. Bashina, *Izv. Akad. Nauk SSSR Neorg. Mater.* **2**(2), 363 (1966).
106. F. E. Wagstaff and K. J. Richards, *J. Am. Ceram. Soc.* **48**(7), 382 (1965).
107. U.S. Pat. 3,370,921 (Feb. 27, 1968), F. E. Wagstaff.
108. D. R. Uhlmann, J. F. Hays, and D. Turnbull, *Phys. Chem. Glasses* **7**(5), 159 (1966).
109. R. C. Yalman and J. F. Corwin, *J. Phys. Chem.* **61**, 1432 (1957).

110. R. H. Doremus, *J. Phys. Chem.* **80**(16), 1773 (1973).
111. R. H. Doremus, *Glass Science*, John Wiley & Sons, Inc., New York, 1973, pp. 121–176.
112. G. H. Frishat, *Ionic Diffusion in Oxide Glasses*, Trans Tech Publications, Bay Village, Ohio, 1975.
113. J. S. Rothman and co-workers, *J. Am. Cer. Soc.* **65**(11), 578 (1982).
114. H. Wakabayashi and M. Tomozawa, *J. Am. Cer. Soc.* **72**(10), 1850 (1989).
115. C. Hetherington and K. H. Jack, *Phys. Chem. Glasses* **5**(5), 147 (1964).
116. C. H. Frischat, *J. Am. Ceram. Soc.* **51**(9), 528 (1968).
117. G. S. Nakayama and J. F. Shackelford, *J. Non-Cryst. Solids* **126**, 249 (1990).
118. R. H. Doremus, *Glass Science*, John Wiley & Sons, Inc., New York, 1973, pp. 121–145.
119. J. Kirchoff and co-workers, *J. Non-Cryst. Solids* **181**, 266 (1995).
120. *TAFQ*, Thermal American Fused Quartz Co., Montville, N.J., 1980.
121. J. F. Shackelford, J. S. Masaryk, and R. M. Fulrath, *J. Am. Cer. Soc.* **53**(7), 417 (1970).
122. A. F. Wells, *Structural Inorganic Chemistry*, Oxford University Press, U.K., 1967, p. 785.
123. P. W. Bridgman and I. Simon, *J. Appl. Phys.* **24**(4), 405 (1953).
124. R. Roy and H. M. Cohen, *Nature* (*London*) **190**, 798 (1961).
125. E. B. Christiansen, S. S. Kistler, and W. B. Gogarty, *J. Am. Ceram. Soc.* **45**(4), 172 (1962).
126. K. Yamana, M. ToKonami, and A. Nakano, *J. Cer. Soc. Jpn.* **98**(4), 311 (1990).
127. S. Yamagata and co-workers, *J. Cer. Soc. Jpn.* **100**(1), 13 (1992).
128. W. Jin, R. Kalia, and P. Vashista, *Phys. Rev.* **B50**(1), 118 (1994).
129. J. D. Mackenzie, *J. Am. Ceram. Soc.* **46**(10), 461 (1963).
130. R. J. Hemsley, H. K. Hao, and P. M. Bell, *Phys. Rev. Lett.* **57**, 747 (1986).
131. C. Meade, R. J. Hemsley, and H. K. Mao, *Phys. Rev. Lett.* **69**, 1387 (1992).
132. W. Primak, L. H. Fuchs, and D. Day, *J. Am. Ceram. Soc.* **38**, 135 (1955).
133. N. F. Borrelli, C. Smith, D. C. Allan, and T. P. Seward III, *J. Opt. Soc. Am. B* **14**(7), 1606 (1997).
134. S.-Y. Hsich and co-workers, *J. Non-Cryst. Solids* **6**, 37 (1971).
135. C. K. Van Peski, R. Morton, and Z. Bor, *J. Non-Cryst. Solids* **265**, 285 (2000).
136. C. M. Smith, N. F. Borrelli, J. J. Price, and D. C. Allan, *Appl. Phys. Lett.* **78**(17), 2452 (2001).
137. J. E. Shelby, *J. Non-Cryst. Solids* **349**, 331 (2004).
138. C. Hetherington, K. H. Jack, and J. C. Kennedy, *Phys. Chem. Glasses* **5**, 130 (1964).
139. V. Zandian, J. S. Florry, and D. Taylor, *J. Br. Cer. Soc.* **90**(2), 59 (1991).
140. *Dynasil Fused Silica*, Dynasil Corp. of America, Berlin, N.J., 1992.
141. *Fused Quartz Tubing*, General Electric Co., Cleveland, Ohio, 1990.
142. *Optical Fused Quartz and Fused Silica*, Heraeus-Amersil, Inc., Sayreville, N.J., 1981.
143. Ref. 7, pp. 218–222.
144. E. H. Fontana and W. A. Plummer, *Phys. Chem. Glasses* **7**, 139 (1966).
145. R. Bruckner, *Glastech. Ber.* **37**(9), 413 (1964).
146. D. W. Bowen and R. W. Taylor, *Ceram. Bull.* **57**(9), 818 (1978).
147. R. Bruckner, *Glastech. Ber.* **37**(10), 459 (1964).
148. T. A. Hahn and R. K. Kirby, in M. C. Craham and H. E. Hagy, eds., *Thermal Expansion*, American Institute of Physics, New York, 1972, pp. 13–24.
149. J. W. Berthold and S. F. Jacobs, *Appl. Opt.* **15**(10), 2344 (1976).
150. H. E. Hagy, *Appl. Optics* **12**(7), 1440 (1973).
151. Ref. 2, p. 311.

152. D. N. Casey and co-workers, *Phys. Chem. Glasses* **17**, 77 (1976).
153. J. C. Lasjaunias and co-workers, *J. Phys. Lett.* **41**, L131 (1980).
154. L. C. K. Carwile and H. J. Hoge, *U.S. Army Technical Report*, 67-7-PR, U.S. Army Natick Laboratories, Natick, Mass., 1966.
155. Ref. 100, p. 627.
156. Ref. 7, pp. 228–230.
157. S. Spinner, *J. Am. Chem. Soc.* **45**, 394 (1962).
158. W. B. Hillig, in J. D. Mackenzie, ed., *Modern Aspects of Vitreous State*, Vol. 2, Butterworth & Co., Washington, D.C., 1962, p. 190.
159. I. Naray-Szabo and J. Ladik, *Nature* (*London*) **188**, 226 (1960).
160. J. C. Morley, P. A. Andrews, and I. Whitney, *Phys. Chem. Glasses* **5**, 1 (1964).
161. W. B. Hillig, *Proceedings of Symposium on the Strength of Glasses and the Means to Improve It*, Union Scientifique Continentale du Verre, Charleroix, Belgium, 1962, p. 206.
162. W. B. Hillig, *J. Appl. Phys.* **32**, 741 (1961).
163. M. L. Hammond and S. F. Ravity, *J. Am. Ceram. Soc.* **46**(7), 329 (1963).
164. S. M. Wiederhorn, *J. Am. Ceram. Soc.* **52**, 99 (1969).
165. J. J. Mecholsky and co-workers, *J. Am. Ceram. Soc.* **57**, 440 (1974).
166. Ref. 7, pp. 210–211.
167. S. M. Wiederhorn, in J. B. Wachtman, ed., *Mechanical and Thermal Properties of Ceramics*, National Bureau Studies Special Publication #303, National Bureau of Standards, Washington, D.C., 1969, p. 217.
168. Annual ASTM Standards, Pt. 17, American Society for Testing and Materials, Philadelphia, Pa., 1978, p. 750.
169. J. H. Westbrook, *Phys. Chem. Glasses* **1**, 32 (1960).
170. J. D. Mackenzie, *J. Am. Ceram. Soc.* **43**, 615 (1960).
171. C. R. Kurkjian, G. W. Kammlott, and M. Munawar Chaudhri, *J. Am. Cer. Soc.* **78**(3), 737 (1995).
172. M. D. Fagan, *Proc. Natl. Electron. Conf.* **7**, 380 (1951).
173. O. L. Anderson and H. E. Bömmel, *J. Am. Ceram. Soc.* **38**, 125 (1955).
174. J. T. Krause, *J. Appl. Phys.* **42**(8), 3035 (1971).
175. E. W. J. Mitchell and E. G. S. Paige, *Philos. Mag.* **1**(8), 1085 (1956).
176. V. Jain, A. K. Varshneya, and P. P. Bihuniak, *Glastech. Ber.* **61**(11), 321 (1988).
177.
178. D. W. Shin and M. Tomozawa, *J. Non-Cryst. Solids* **161**, 203 (1993).
179. A. E. Owens and R. W. Douglas, *J. Soc. Glass Tech.* **43**, 159 (1959).
180. D. Grischkowsky, S. Keiding, M. van Exter, and Ch. Fattinger, *J. Opt. Soc. Am. B* **7**(10), 2006 (1990).
181. G. L. Tan, M. F. Lemon, D. J. Jones, and R. H. French, *Phys. Rev. B* **72**, 205117 (2005).
182. W. Weyl, *Coloured Glasses*, Society of Glass Technology, Sheffield, England, 1986.
183. G. H. Sigel, Jr., *J. Non-Cryst. Solids* **13**, 372 (1973).
184. L. Skuja, *J. Non-Cryst. Solids* **239**, 16 (1998).
185. H. Mohn, *60 Jahre Quartzglas-25 Jahre Hochvakuumtechnik*, W. C. Heraeus GmbH, Hanau, Germany, 1965, p. 114.
186. G. Hetherington, K. H. Jack, and M. W. Ramsay, *Phys. Chem. Glasses* **6**(1), 6 (1965).
187. V. Garino-Canina, *Verres Refrac.* **6**, 313 (1958).
188. L. Dong and co-workers, *J. Opt. Soc. Am.* **B11**(10), 2106 (1994).
189. R. V. Adams and R. W. Douglas, *J. Soc. Glass Tech.* **43**, 147 (1959).
190. C. J. Parker, technical data, Corning Glass Works, Corning, N.Y., 1956.
191. W. A. Clayton, *Space Aeronaut.* 129 (June 1963).
192. I. H. Malitson, *J. Opt. Soc. Am.* **55**, 1205 (1965).

193. B. Brixner, *J. Opt. Soc. Am.* **57**(5), 674 (1967).
194. G. Hetherington and K. H. Jack, *Phys. Chem. Glasses* **3**(4), 129 (1962).
195. C. M. Smith and L. A. Moore, *J. Fluor. Chem.* **122**, 81 (2003).
196. R. Brückner, *Glastech. Ber.* **37**, 459 (1964); **38**, 153 (1965).
197. J. W. Fleming Jr. and J. W. Schiever, *J. Am. Cer. Soc.* **62**(9–10), 526 (1979).
198. R. M. Waxler and G. W. Cleek, *J. Res. NBS-A. Phys. Chem.* **75**(4), 279 (1971).
199. E. Lell, N. J. Kreidl, and J. R. Hensler, in J. Burke, ed., *Progress in Ceramic Science*, Vol. 4, Pergamon Press, Inc., New York, 1966.
200. M. C. Wittels and F. A. Sherrill, *Phys. Rev.* **93**, 1117 (1954).
201. I. Simon, *J. Am. Ceram. Soc.* **41**, 116 (1958).
202. G. Mayer and M. Lecomte, *J. Phys. Rad.* **21**, 846 (1960).
203. A. E. Clark and R. E. Strakna, *Phys. Chem. Glasses* **3**, 121 (1962).
204. A. F. Cohen, *J. Appl. Phys.* **29**, 591 (1958).
205. W. Primak, *Phys. Rev.* **110**, 1240 (1958).
206. F. L. Galeener and co-workers, in Ref. 24, p. 284.
207. G. W. Arnold, Jr., *J. Phys. Chem. Solids* **13**, 306 (1960).
208. Ref. 199, pp. 3–93.
209. P. H. Caskell and D. W. Johnson, *J. Non-Cryst. Solids* **20**, 153, 171 (1976).
210. D. L. Griscom, in Ref. 24, p. 232.
211. E. Lell, *Phys. Chem. Glasses* **3**, 84 (1962).
212. J. M. Stevels, in V. D. Frechette, ed., *Non-Crystalline Solids*, John Wiley & Sons, Inc., New York, 1960, pp. 412–441.
213. A. J. Cohen, *J. Chem. Phys.* **23**, 765 (1955).
214. P. W. Levy, *Phys. Chem. Solids* **13**, 287 (1960).
215. O. Kittelmann and J. Ringling, *Optics Lett.* **19**(24), 2053 (1994).
216. S. Faile and R. Roy, *Mater. Res. Bull.* **5**, 385 (1970).
217. R. J. Araujo, N. F. Borrelli, and C. M. Smith, *Inorganic Optical Materials*, Proceedings of SPIE Vol. 3242, 1998, pp. 2–9.
218. M. Rothschild, D. J. Ehrlich, and D. C. Shaver, *Appl. Phys. Lett.* **55**, 1276 (1989).
219. R. E. Schenker and W. G. Oldham, *J. Appl. Phys.* **82**, 1065 (1997).
220. Technical data, Sylvania Emissive Products, Portsmouth, N.H., 1985.
221. S. G. Hurt and co-workers, *Chromatogr. News* **8**(2), 32 (1980).
222. R. A. Ragatz and O. A. Hougen, *Chem. Met. Eng.* **33**, 415 (1926).
223. Ref. 185, pp. 174–177.
224. Technical data, NSG Precision Cells, Farmingdale, N.Y., 1992.
225. D. C. Ferranti, *Microelecto. Manufactur. Test.* 18–20 (Apr. 1989).
226. *Introduction to Microlighography*, in L. F. Thompson, C. G. Willson, M. J. Bowden, eds., American Chemical Society, Washington, D.C., 1995.
227. G. Sucki, *Energy Technology Review*, Lawrence Livermore National Laboratories, Livermore, Calif., Apr./May, 1986, pp. 28–33.
228. J. W. McBain and A. M. Baker, *J. Am. Chem. Soc.* **48**, 690 (1926).
229. P. Hidnert and W. Sauder, *Natl. Bur. Std.* (*U.S.*) Circ. 486 (1950).
230. E. W. Beggs, *Illum. Eng.* **42**, 435 (1947).
231. H. D. Frazer and W. S. Till, *Illum. Eng.* **47**, 207 (1952).
232. D. A. Larson and co-workers, *Illum. Eng.* **58**, 434 (1963).
233. E. C. Martt, L. J. Smialek, and A. C. Green, *Illum. Eng.* **59**, 34 (1964).
234. J. R. Fitzpatrick and V. W. Goddard, *J. Illum. Eng. Soc.* **10**(2), 107 (1981).
235. Ger. Offen. 2,524,410 (Dec. 11, 1975), E. M. Clausen (to General Electric Co.).
236. U.S. Pat. 3,988,628 (June 13, 1974), E. M. Clausen (to General Electric Co.).
237. U.S. Pat. 3,879,625 (Oct. 9, 1973), C. I. McVey and O. M. Uy (to General Electric Co.).
238. J. A. Moore and C. M. Jolly, *Gen. Electr. Corp. J.* **29**, 99 (1962).
239. T. M. Lemons and E. R. Meyer, *Illum. Eng.* **59**, 723 (1964).

240. E. B. Shand, *Glass Engineering Handbook*, McGraw-Hill Book Co., Inc., New York, 1958, pp. 354–355.
241. K. M. Eisele and R. Ruthardt, *J. Electrochem. Soc.*: *Solid-State Sci. Technol.* **125**(7), 1188 (1978).
242. *T07 Stabilized Diffusion Tubes*, Heraeus-Amersil, Sayreville, N.J., 1980.
243. *Photomask Substrates for Microlithography*, Corning Glass Works, Corning, New York, 1980.
244. H. A. Miska, *Engineering Materials Handbook*, Vol. 4, *Ceramics and Glasses*, ASM International, Metals Park, Ohio, 1991.
245. C. J. Parker, *Appl. Opt.* **7**, 740 (1968).
246. C. L. Rathmann, C. H. Mann, and M. E. Nordberg, *Appl. Opt.* **7**, 819 (1968).
247. Ref. 185, pp. 143–149.
248. *Ceramics Ind.* **143**(5), 36 (Oct. 1994).
249. R. R. Johnson, *Opt./Photon. News* **6**(3), 16 (Mar. 1995).
250. *Corguide Optical Fiber*, Corning Inc., Corning, N.Y., 1990.
251. T. C. Starkey, *Photonics Spectra* **23**(3), 119 (Mar. 1989).
252. C. M. Smith and co-workers, *Nature* (*London*) **424**, 657 (2003).
253. R. Cregan and co-workers, *Science* **285**, 1537 (1999).
254. D. C. Allan and co-workers, *Photonic Crystals and Light Localization in the 21st Century*, in C. M. Soukoulis, ed., Kluwer Academic, Dordrecht, 2001, pp. 305–320.
255. Technical data, Cabot Corp., Boston, Mass., 1974.
256. J. J. Miller and D. L. Eppink, *Leaching of Preformed Ceramic Cores*, Sherwood Refractories, Inc., Cleveland, Ohio, 1977.
257. H. G. Floch and J. J. Priotton, *Ceramic Bull.* **69**(7), 1141 (1990).

CHARLENE M. SMITH
Corning Incorporated

Table 1. **Classification of Commercial Vitreous Silicas**

Type	Method	Impurities, ppm			Representative glasses
		OH	Cl	Cations	
I	electric melting of quartz	<20	0	50–300	Infrasil, Vitreosil-ir, GE-124, GE-214
II	flame fusion of quartz	200–500	0	10–50	Homosil, Optosil, Vitreosil-O55
III	flame hydrolysis	600–1200	50–100	<1	Corning 7980, Dynasil 1000, Shinetsu P-10, Spectrosil, Suprasil, NSG-ES
IV	oxidation of $SiCl_4$ (plasma)	<20	<200	1–2	Spectrosil WF, Suprasil-W
V	sol–gel	<1	<1–500	<1	GELSIL

Table 2. **Impurity Concentrations in Vitreous Silicas**[a]

Impurity, ppm	Translucent vitreous silica	Transparent vitreous silica[b]		
		Type I	Type II	Type III[c]
aluminum	18–176	16	10–50	<0.05
antimony	<0.06	0.3	0.15	<0.005
arsenic	<0.01	<0.4	0.08	<0.005
boron	<0.1	<0.1	0.1	0–0.01
calcium	2.0	0.6	0.8–3.0	<0.1
chromium	<0.09	<0.01	1–2.0	<0.03
cobalt		0.05		0.01
copper	<0.15	<0.1	0.7	0.004
gallium			0–0.008	<0.02
gold	<0.03		0.0003	
hydroxyl	<200	<5	~180	<1250
iron	1	0.3	0.8	<0.12
lithium	1.3	1.0	0–2.0	<0.001
magnesium	0.1	0.1	0.2	<0.05
manganese	0.1	0.1	0.01	<0.01
mercury				<0.01
phosphorus	0.1–1.5	1.5	0.1	<0.001
potassium	1.0	0.7	0.8	<0.1
sodium	2.0–3.0	1.0	1.0	<0.1
titanium	1.1–63	1.1	0.8	<0.04
uranium	<0.04		0.0003	<0.001
zinc				<0.03
zirconium	1.0–1.5	1.5	0–0.1	<0.03

[a]Data taken from manufacturers' publications.
[b]See Table 1 classifications.
[c]The metallic impurities of Type IV vitreous silica are similar to those of Type III material, except for a negligible hydroxyl content.

Table 3. **Corrosion Rates of Vitreous Silica in Aqueous Media**[a]

Solution[b]	Temperature, °C	Duration of test, h	Weight loss, mg/cm^2
	Alkaline solutions		
NH_4OH, 10%	20	100	0.019
NaOH			
10%	18	100	0.031
5%	95	6	0.7
8%	100	10	1.21
KOH			
30%	18	100	0.027
10.2%	100	10	1.13
Na_2CO_3			
5%	18	100	0.0015
10%	100	10	0.37
	Acid solutions		
acetic acid, 70%	108	24	0.1
hydrochloric acid			
5%	95	24	<0.01
$\rho = 1.19$	66	24	1.4
nitric acid, $\rho = 1.40$	115	24	1.1
sulfuric acid			
5%	95	24	<0.01
$\rho = 1.84$	205	24	0.6
phosphoric acid	300	15	580

[a]Refs. 87 and 90.
[b]ρ = density in g/mL.

Table 4. **Dissolution Rates of Silica Phases**[a]

	Silica dissolved, %	
Silica phase[b]	In 5% HF, 1/2 h	In 1% HF, 1 h
quartz	30.1	5.2
tridymite	76.3	20.3
cristobalite	74.3	25.8
vitreous silica	96.6	52.9

[a]Ref. 93.
[b]Samples of uniform particle size, ~40-μm diameter.

Table 5. **Diffusion Coefficients in Vitreous Silica**[a]

Metal	Ion	D at 1000°C, cm^2/s
lithium	Li^+	1×10^{-6}
sodium	Na^+	7.9×10^{-6}
potassium	K^+	$(5–10) \times 10^{-8}$
rubidium	Rb^+	$(1.4–3.2) \times 10^{-10}$
cesium	Cs^+	9×10^{-11}
calcium	Ca^{2+}	2×10^{-8}
aluminum	Al^{3+}	1×10^{-13}
nickel	Ni^{2+}	1×10^{-15}

[a]Refs. 111–113.

Table 6. **Diffusion in Vitreous Silica**[a]

Gas	Diameter, pm	D at 1000°C, cm^2/s	Activation energy, kJ/mol[b]
helium	200	5.5×10^{-5}	20
neon	240	2.5×10^{-6}	37
hydrogen	250	7.3×10^{-6}	36
argon	320	1.2×10^{-9}	113
oxygen	320	6.6×10^{-9}	105
nitrogen	340		110
krypton	420		~190
xenon	490		~300
fluorine		3.3×10^{-16}	383
chlorine		6.2×10^{-13}	211

[a]Refs. 117–119.
[b]To convert J to cal, divide by 4.184.

Table 7. **Viscosity Data**[a]

Parameter	Quartz Syndicate, Inc.			Vitreosil				
	Transparent	Translucent	G.E.-204	ir	OG[b]	Heraeus Supersil	Corning 7940	Dynasil
silica type	I	I	II	II	I	III	III	III
OH, ppm			low	3	400	1200	900–1000	600–1000
softening point, °C	1670	1650	1813	1582	1597	1600	1585	1600 ± 25
annealing point, °C	1140	1100	1213	1190	1108	1075	1075	1100 ± 20
strain point, °C	1070	1040	1107	1108	1015	987	990	1000 ± 20

[a]Data from manufacturers' product literature; data for Vitreosil from Ref. 138.
[b]OG = optical grade.

Table 8. **Dielectric Properties of Synthetic Fused Silica**[a]

	Frequency, Hz		
Parameter, °C	100	1,000	10,000
dielectric constant			
25	3.79	3.79	3.79
200	3.81	3.81	3.81
300	3.82	3.82	3.82
400	3.85	3.83	3.82
loss factor			
25	0.00002	0.00002	0.00002
200	0.00052	0.00012	0.00004
300	0.08	0.0072	0.00072
400	1.0	0.2	0.022

[a]Ref. 87.

Table 9. **Hydroxyl Concentration of Vitreous Silicas**

Manufacturer	Material name	UV curve[a]	IR curve[a]	β_{OH}, ppm
Corning Incorporated	Code 7980	1	A	800–1000
	Code 7943	3	C	<1
	Code 7957	1	C	<1
Dynasil Corp. of America	Dynasil			
	Petrosil[b]	1	A	<1000
	QIR	3	C	<0.1
	QUV	2	B	150–180
	QVIS, QZ	3	B	150–180
	SWF	2	C	5
	SUV	1	A	1200–1500
General Electric Co.	Types 214 rods	2	C	<5
	Types 124 ingots	3	C	<10
Heraeus Amersil Inc.	Ultrasil	2	B	180
	Homosil, Optosil	3	B	180
	Infrasil	3	C	<8
	Suprasil-W1, W2	1	C	5
	Suprasil 1,2,3	1	A	900–1200
	Suprasil 300	1	C	<1
	Suprasil 311, 312	1	C	200
Nippon Silica Glass	ES	1	A	1200
	IR	3	C	<8
	SG, OX	3	B	150
Quartz & Silice[c] (Thermal American Fused Quartz)	Spectrosil A, B	1	A	1000
	Spectrosil WF	1	C	
	Vitreosil ir	3	C	
Shinetsu Quartz (JV with Heraeus)	Suprsil P10, 20, 30	1	A	1200
SumiQuartz (Sumitomo)	SK-1300	1	B	150
Westdeutsche Quarzschmelze GmbH	Synsil	1	A	

[a]See Fig. 7.
[b]Petrosil is manufactured in Russia.
[c]Quartz & Silice, Quartz Products Co., and Thermal Quartz Schelze GmbH are Saint-Gobain Group Companies.

Table 10. **Manufacturers and Suppliers of Vitreous Silica**

Company	Location
United States	
A. A. I. Products Inc.	Woodbridge, N.J.
Cabot Corp.	Boston, Mass.
Corning Incorporated	Corning, N.Y.
Dynasil Corp. of America	Berlin, N.J.
GE Quartz Products	Cleveland, Ohio
OSRAM-Sylvania	Exeter, N.H.
Heraeus Amersil Inc.[a]	Duluth, Georgia
J. P. Stevens & Co., Inc.	Greenville, S.C.
Pyromatics, Inc.	Willoughby, Ohio
Quartz Products Co.[b]	Louisville, Ky.
Quartz Scientific, Inc.	Fairport Harbor, Ohio
Outside United States	
Asahi Glass	Tokyo, Japan
Heraeus Quarzglass GmbH	Hanau, Germany
Hitachi Cable	Tokyo, Japan
Iruvisil Co., Ltd.	St. Petersburg, CIS
Fujikura	Tokyo, Japan
Mitsubishi Cable	Itami, Japan
Shin-Etsu Quartz Products Co., Ltd.	Kokai, Japan
SICO	Jena-Burgau, Germany
Sumitomo Electric Industry	Osaka, Japan
Thermal Quarz Schmelze GmbH[a]	Weisbaden, Germany
Thermal Syndicate, Ltd.[b]	Wallsend, U.K.
Toshiba Ceramics	Tokyo, Japan
TOSOH/Nippon Silica Glass	Tokyo, Japan
Quartz & Silice[b]	France, Holland, Italy
Westdeutsche Quarzschmelze GmbH[c]	Munchen, Germany

[a]Subsidiary of Heraeus Quarzglass GmbH.
[b]Subsidiary of Saint-Gobain Group Co. Quartz Technology Division.
[c]Subsidiary of General Electric.

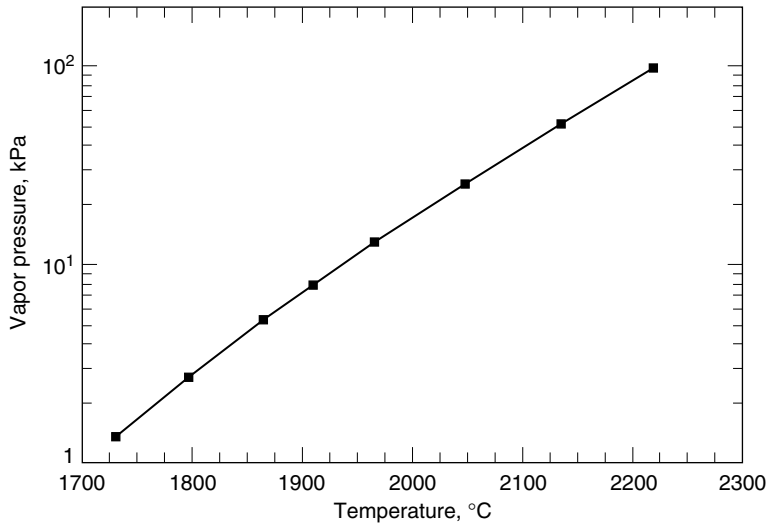

Fig. 1. Vapor pressure of silica at elevated temperatures (98). To convert kPa to psi, multiply by 0.145.

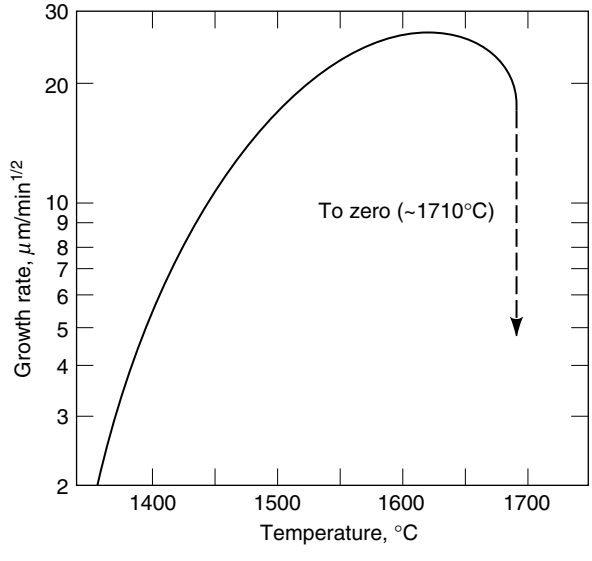

Fig. 2. Devitrification rate of vitreous silica for surface-nucleated cristobalite as a function of temperature (101). Growth rate is proportional to the square root of time. Measurements were made on G.E. fused silica, heat treated in air.

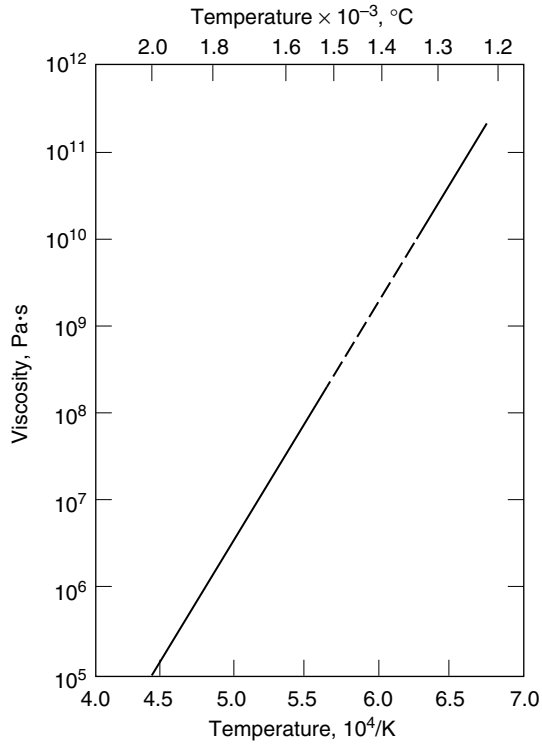

Fig. 3. Viscosity–temperature curve for Amersil commercial-grade silica, where the dashed line represents interpolation between data sets (144,145). 10 Pa·s = 1P.

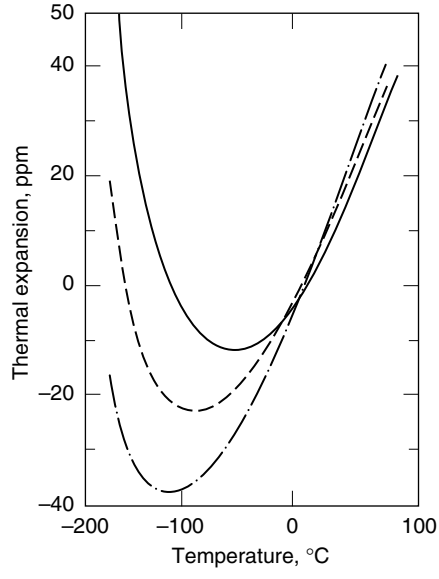

Fig. 4. Effect of thermal history on low temperature thermal expansion of vitreous silica (147), where (–·), (– – –), and (—) represent glasses having fictive temperatures of 1000, 1300, and 1720°C, respectively.

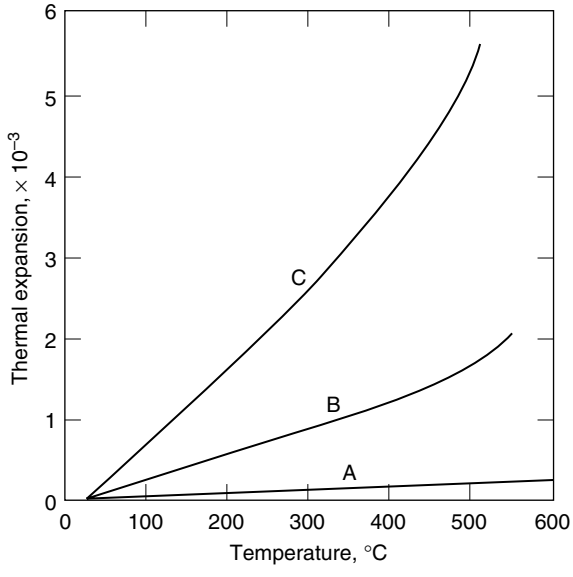

Fig. 5. Comparison of thermal expansion of vitreous silica, A, to that of borosilicate glass, B, and soda–lime glass, C.

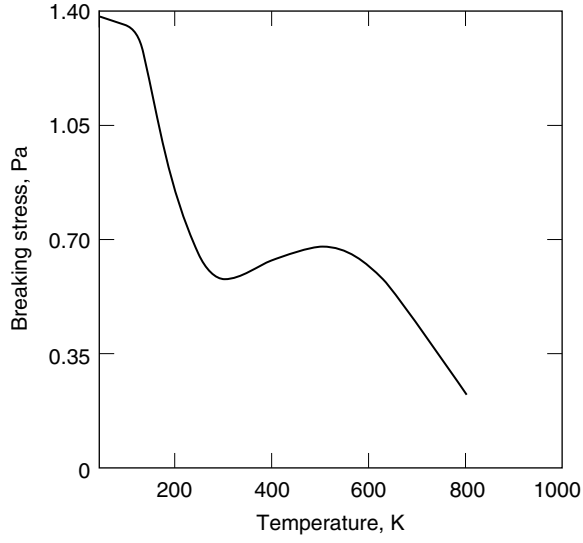

Fig. 6. Effect of temperature on the strength of vitreous silica fiber (160). To convert Pa to mmHg, multiply by 0.0075.

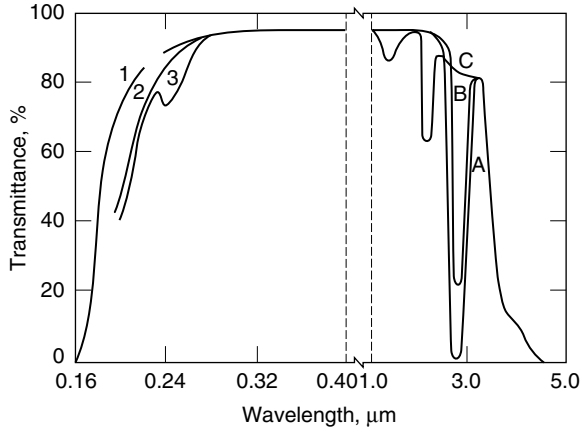

Fig. 7. Transmission curves for vitreous silica, 1-cm thick. See Table 9.

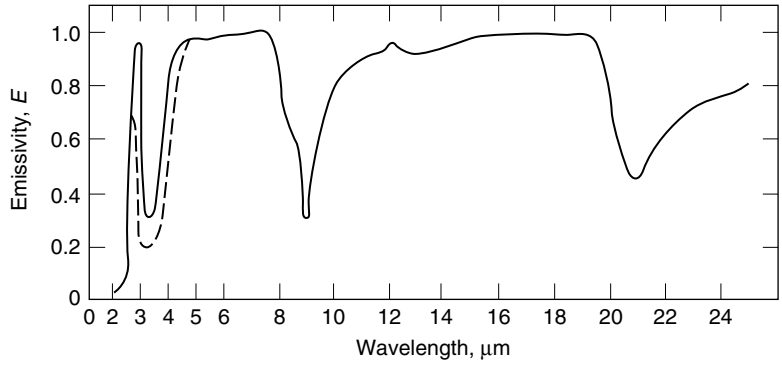

Fig. 8. Special normal emissivity of vitreous silica, where (—) corresponds to a sample 1.27-cm thick and (– – –), 0.64-cm thick (190).

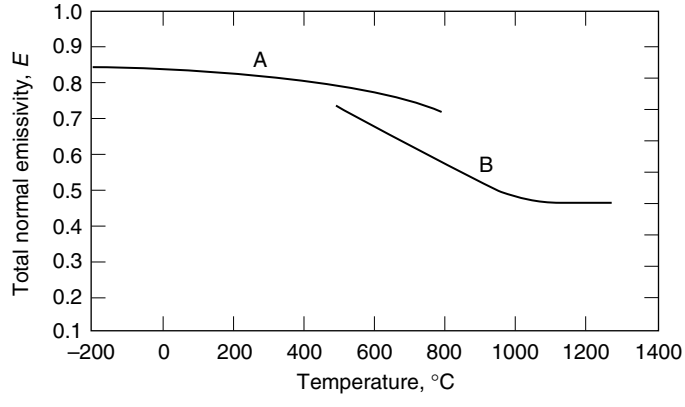

Fig. 9. Total normal emissivity of vitreous silica, where A corresponds to a sample 1.27-cm thick and B, 0.64-cm thick (191).

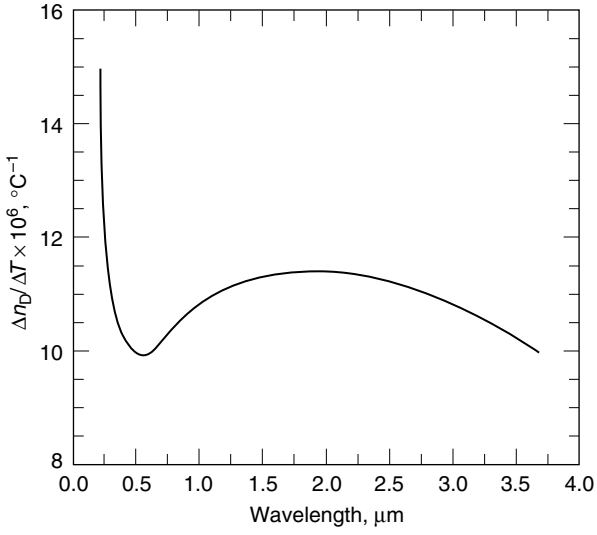

Fig. 10. Thermal coefficient of the refractive index in vitreous silica at $\sim 25^{\circ}$C (192).

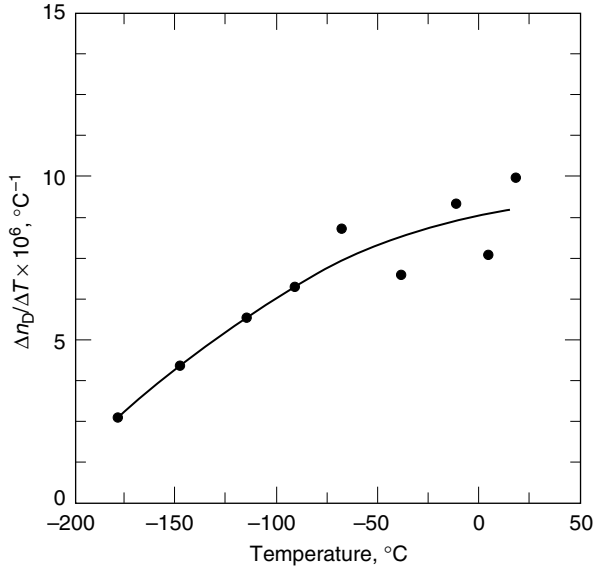

Fig. 11. Change in $\Delta n_D/\Delta T$ with temperature in vitreous silica measured at 587.6 nm (198).

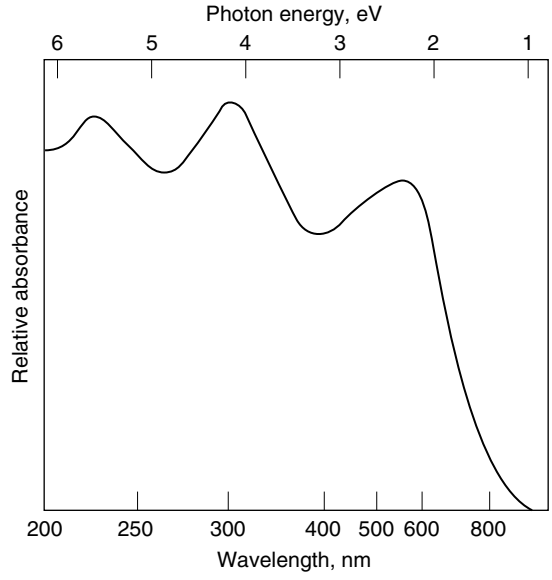

Fig. 12. Absorption spectrum of irradiated impure vitreous silica, Heraeus fused quartz, after a radiation dose of 10^4 Gy (10^6 rad) (212). The main impurity is aluminum.

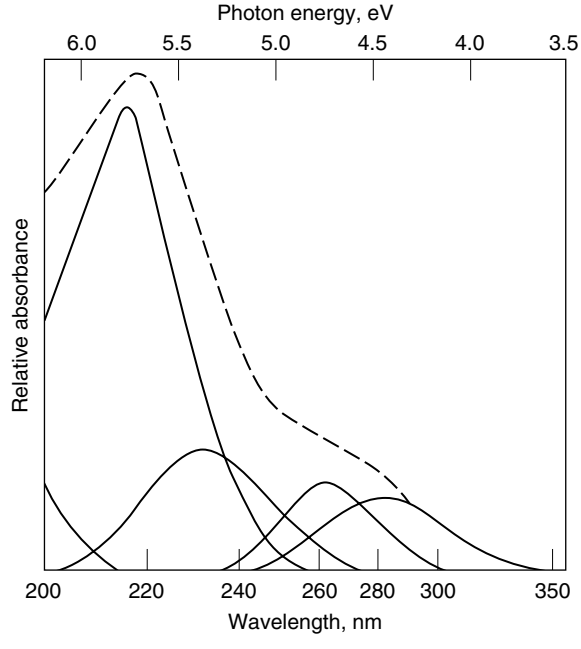

Fig. 13. Total (– – –) absorption spectrum and resolved (—) bands of irradiated high purity vitreous silica (214). Measurements made on Corning Code 7940 glass after a radiation dose of 26 Gy (2600 rad).